Tropospheric ozone and El Niño–Southern Oscillation: Influence of atmospheric dynamics, biomass burning emissions, and future climate change

Tropospheric ozone and El Niño–Southern Oscillation: Influence of atmospheric dynamics, biomass burning emissions, and future climate change

R. M. Doherty,[1] D. S. Stevenson,[1] C. E. Johnson,[2] W. J. Collins,[2] and M. G. Sanderson[2]

Received 3 November 2005; revised 28 February 2006; accepted 13 June 2006; published 5 October 2006.

[1] We investigate how El Niño Southern Oscillation (ENSO) influences tropospheric ozone and its precursors in a coupled climate-chemistry model. As shown in similar studies, tropospheric column ozone (TCO) decreases in the central and east Pacific and increases in the west Pacific/Indonesia in response to circulation and convective changes during El Niño conditions. Simulated changes in TCO for "peak" El Niño events in the central and east Pacific are in good agreement but are underestimated in the west Pacific compared to previous observational and modeling studies for October 1997. Tropospheric column-average NO_x decreases over Indonesia and generally over South America as a result of suppressed convection and lightning over these land regions. NO_x and HO_x changes during El Niño modify ozone chemical production and destruction. When we include annually varying biomass burning emissions in our model simulations we find that these emissions peak over Indonesia 1–2 months in advance of the peak elevated sea-surface temperatures (SSTs) and hence the "meteorological" El Niño. We underestimate the strength of the TCO increase due to El Niño–related dry conditions over Indonesia in October 1997 compared to observations. We also examine how future mean and variability changes in ENSO, as simulated in the HadCM3 climate model, impacts tropospheric ozone. A mean future El Niño–like state is simulated in the tropical Pacific in HadCM3, but this has no discernable impact on the future TCO trend in this region. However, we do simulate increased variability in precipitation and TCO related to ENSO in the future.

Citation: Doherty, R. M., D. S. Stevenson, C. E. Johnson, W. J. Collins, and M. G. Sanderson (2006), Tropospheric ozone and El Niño–Southern Oscillation: Influence of atmospheric dynamics, biomass burning emissions, and future climate change, *J. Geophys. Res.*, *111*, D19304, doi:10.1029/2005JD006849.

1. Introduction

[2] El Niño Southern Oscillation (ENSO) is the dominant mode of interannual variability in tropical climate. It also exerts a major influence on the interannual variability of chemistry in the troposphere. Unprecedented levels of tropospheric ozone were measured, coincident with wildfires over Indonesia during drought conditions induced by the 1997/1998 El Niño event [*Fujiwara et al.*, 1999, 2000; *Thompson et al.*, 2001]. This event heightened interest in the impact of ENSO on tropospheric ozone, and in particular the relative importance of atmospheric dynamics compared to increased biomass burning during El Niño. In the future, changes in climate toward a mean El Niño–like state, with temperatures in the central and eastern Pacific projected to warm more than in the western Pacific and with a corresponding eastward shift in precipitation, has been simulated in several coupled ocean-atmosphere General Circulation Models GCMs [*Cubasch et al.*, 2001]. One or two GCMs have shown an opposing La Niña–like mean trend [*Cubasch et al.*, 2001]. In an evaluation of ~20 GCMs, *Collins* [2005] found no overall model consensus toward a future mean El Niño–like state. Changes in the frequency of ENSO have also been the subject of several GCM studies, again with conflicting results from different GCMs [*Timmermann et al.*, 1999; *Collins*, 2000]. It is important to fully understand the impacts of present-day ENSO on tropospheric composition, in order to evaluate the consequences of possible future changes in ENSO on tropospheric composition. For example, was the 1997/1998 El Niño event and its impact on tropospheric ozone unique, or will we see more such events in the future?

[3] Previous observational and modeling studies examined changes in tropospheric column ozone (TCO) at the peak of the 1997/1998 El Niño–induced biomass burning episode. *Chandra et al.* [1998] derived TCO decreases of 4–8 DU over the east Pacific and 10–20 DU TCO increases over the west Pacific and Indonesia from the Total Ozone Mapping Spectrometer (TOMS) for October 1997. The

[1]Institute of Atmospheric and Environmental Sciences, University of Edinburgh, Edinburgh, UK.
[2]Hadley Centre for Climate Prediction and Research, Met Office, Exeter, UK.

0148-0227/06/2005JD006849

increase in TCO extended over most of the west Pacific well outside the biomass burning region such that the basin-wide pattern of change resembled a west to east dipole about the dateline. They attributed these changes in TCO to a combination of large-scale circulation processes associated with the shift in the tropical convection pattern, and surface/boundary layer processes due to forest fires in the Indonesian region. The changes in large-scale circulation caused TCO decreases associated with enhanced convection and upward motion of low ozone air from the lower troposphere, and TCO increases associated with suppressed convection and downward motion of high ozone air from the upper troposphere. Similar TCO changes were simulated for October 1997 in modeling studies by *Sudo and Takahashi* [2001], *Chandra et al.* [2002] and *Zeng and Pyle* [2005]. Modeling studies to investigate the importance of biomass burning versus changes in meteorological conditions suggest that both mechanisms contributed almost equally to the observed increase in TCO in the Indonesian region in 1997/1998 [*Chandra et al.*, 2002; *Sudo and Takahashi*, 2001]. The effect of biomass burning emissions on ozone production was largely confined to the lower troposphere (LT) as a result of suppressed convection.

[4] *Chandra et al.* [1998] also examined TCO changes during the peak of the 1982/1983 El Niño event. Unlike 1997, they found comparable TCO decreases in the east Pacific and increases in the west Pacific (4–8 DU). A few further studies examined ENSO-induced tropospheric ozone changes over longer periods (1–2 decades) [*Ziemke and Chandra*, 1999, 2003; *Peters et al.*, 2001]. Using a regression model on 20 years of TOMS TCO, *Ziemke and Chandra* [1999] calculated annual-average positive and negative anomalies both of 3–4 DU associated with El Niño events over the 1979–1999 period, which explained ~40% of the interannual variability. *Peters et al.* [2001] simulated similar magnitudes of change for deseasonalized monthly ENSO (El Niño and La Niña) events during 1979–1993 but with 25% interannual variability explained by ENSO. Further regression model studies of deseasonalized monthly TOMS TCO by *Ziemke and Chandra* [2003] yielded larger changes of 5 DU and higher in the east and west Pacific (see their Figure 4) for an average of the 4 major El Niño and 3 La Niña events during 1970–2001. Therefore the large enhancement over Indonesia during the El Niño–induced biomass burning event 1997/1998 seems to have been unique [*Peters et al.*, 2001].

[5] ENSO-related changes in atmospheric chemistry that affect tropospheric ozone production have been investigated. In situ ozone formation occurs by oxidation of carbon monoxide and hydrocarbons in the presence of nitrogen oxides (NO_x = NO + NO_2). The main ozone production reaction is NO + HO_2 → NO_2 + OH and subsequent rapid NO_2 photodissociation. Ozone destruction occurs mainly through photolysis followed by reaction of the liberated oxygen atom with water vapor: $O(^1D) + H_2O \rightarrow 2OH$. Isoprene ($C_5H_8$) is a higher hydrocarbon emitted by some types of vegetation that can promote ozone production through production of HO_2 radicals, if the local levels of NO_x are sufficiently high. Biogenic isoprene emissions are strongly temperature sensitive [*Sanderson et al.*, 2003b]. *Sudo and Takahashi* [2001] suggested that changes in convection affected tropospheric ozone loss rates and lifetime, as well as NO_x through wet scavenging of HNO_3 and OH changes. Generally, as with ozone, NO_x decreased through the troposphere (reducing ozone production) with enhanced convection, and increased (enhancing ozone production) in regions of suppressed convection. Small areas of NO_x decrease over the region of suppressed convection in the upper troposphere (UT) were attributed to a reduction in lightning NO_x emissions. Using the same coupled model as used in this study (HadAM3-STOCHEM) we previously demonstrated that interannual variations in global isoprene and lightning NO_x emissions were strongly influenced by ENSO [*Stevenson et al.*, 2005]. *Zeng and Pyle* [2005] found that ENSO also influenced tropospheric ozone through modulation of the net flux of stratospheric ozone into the troposphere (STE). The STE response was most prominent 6 months after the peak of the ENSO event. Variability in the methane accumulation rate was found to be influenced by ENSO through changes in water vapor and OH [*Johnson et al.*, 2002].

[6] In this paper we use several versions of a coupled climate-chemistry model to explore the influence of present-day ENSO on tropospheric composition, and assess the influence of interannual variability of biomass burning emissions over the period 1980–2000. The influence of future changes in ENSO variability on tropospheric ozone is then investigated. Section 2 discusses the models, simulations performed and analytical techniques. Section 3 describes the meteorological influence of ENSO on tropospheric ozone, and section 4 the biomass burning impact. Section 5 explores future ENSO variability and section 6 presents discussions and conclusions.

2. Methodology

[7] In this section we describe the models used, the experiments performed and the analytical techniques carried out.

2.1. Models

[8] We use two versions of the Hadley Centre GCM: HadAM3 and HadCM3 coupled to the Lagrangian chemistry transport model STOCHEM [*Stevenson et al.*, 2004]. HadAM3 is an atmospheric GCM [*Pope et al.*, 2000] which is driven by prescribed sea-surface temperatures (SSTs), and is used here for studying present-day ENSO. Results from HadCM3 [*Johns et al.*, 2003], which is a coupled ocean-atmosphere GCM (not flux-adjusted), are used in this study to examine future changes in ENSO. HadAM3 and HadCM3 were run at standard resolution for the atmosphere of 3.75° longitude by 2.5° latitude, with 19 vertical levels extending to ~10 hPa. The STOCHEM model version used in this study has been described by *Sanderson et al.* [2003a, 2003b], *Stevenson et al.* [2004] and *Doherty et al.* [2005]. As a Lagrangian model, its atmosphere is divided into 50,000 air parcels that are advected by HadAM3/HadCM3 winds. Air parcels are mapped onto a 5° by 5° horizontal grid with 9 equally spaced vertical layers which extend to 100 hPa. In specifying an upper lid on the chemistry model at 100 hPa, we miss a small fraction of the upper tropical troposphere, and we estimate this will lead to a small (<10%) underestimate in TCO in our calculations. Stratospheric ozone influx comes from the *Li and Shine* [1995]

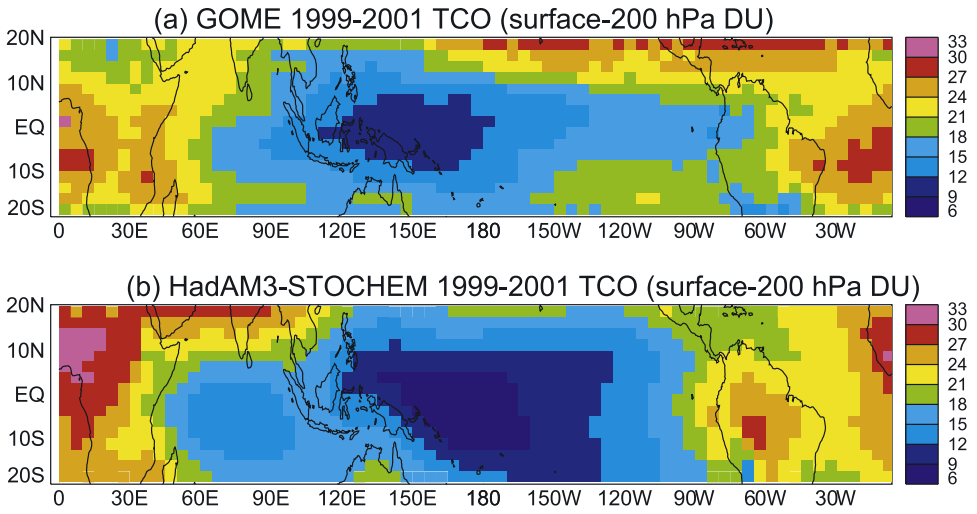

Figure 1. Annual-average (a) observed and (b) HadAM3-STOCHEM tropical TCO (surface to 200 hPa), in DU, averaged over the period 1999–2001. Observations are from the GOME satellite, and the time period includes some missing data at some locations; the model results have been sampled in exactly the same way, to exclude any sampling bias.

stratospheric ozone climatology distributed into the troposphere by vertical winds at STOCHEM's upper boundary of 100 hPa. By using an ozone climatology at 100 hPa, we ensure that descending air has realistic ozone values, and that the model reasonably represents global STE of ozone, however we preclude simulation of any climate-related influences on ozone concentrations above this level. Climate-related influences on the STE mass flux (i.e., winds), however, will be represented.

[9] There are several updates to the STOCHEM model coupled to HadAM3 compared to the version coupled to HadCM3. Since these updates are described in previous papers, only changes that are relevant to ENSO are discussed here. These include updates to the convective mixing, lightning NO_x emissions and biogenic isoprene schemes. Note that although the convective mixing schemes in the two versions of STOCHEM differ, the convection scheme represented in the two climate models HadAM3 and HadCM3 is identical. In the HadAM3-STOCHEM coupled integrations, STOCHEM uses the *Collins et al.* [2002] convective mixing scheme, which is based on 3D convective mass updraught fluxes generated in HadAM3 [*Gregory et al.*, 1997]. In HadCM3-STOCHEM an older convective mixing scheme is used, based on convective precipitation rate and cloud top height [*Stevenson et al.*, 1998]. *Collins et al.* [2002] compared the two convection schemes, and found that both schemes have a similar effect on ^{222}Rn profiles despite using very different approaches. In HadAM3-STOCHEM, emissions of lightning NO_x are coupled to convection according to *Price et al.* [1997] and are vertically distributed using the *Pickering et al.* [1998] profiles; in HadCM3-STOCHEM lightning NO_x emissions have a seasonal but annually invariant 3D spatial distribution and are not directly linked to convection fields. Another difference is that isoprene emissions in HadAM3-STOCHEM are linked to vegetation, radiation and temperature, while in HadCM3-STOCHEM these emissions have a seasonal but annually invariant spatial distribution. The global production of lightning NO is scaled to be roughly 7 Tg N yr^{-1} and global isoprene emissions are 575 Tg yr^{-1} in HadAM3-STOCHEM; these compare with totals of 5 Tg N yr^{-1} and 506 Tg yr^{-1} in HadCM3-STOCHEM. The surface deposition scheme has also been updated [*Sanderson et al.*, 2003a]. Other aspects of the chemical transport scheme are unchanged. The 20-year mean tropospheric O_3 budget for these HadAM3-STOCHEM simulations is given by *Doherty et al.* [2005].

[10] Evaluation of simulated and observed ^{222}Rn profiles has been performed by *Collins et al.* [2002], however not over the tropics because of a lack of observations. Convective mass fluxes from HadAM3 and ERA-40 analyses have been compared by *Doherty et al.* [2005]. These suggest good agreement in terms of spatial distributions but the strength and height of convection are larger in HadAM3. Validation of HadAM3-STOCHEM results against ozonesonde observations of O_3 and NO_x have been performed by *Stevenson et al.* [2004], *Dentener et al.* [2005] and *Doherty et al.* [2005]. There is a tropical model bias to underestimate NO_x in the UT and overestimate NO_x in the LT, and to underestimate O_3 in the lower to midtroposphere (MT). However, model results generally fall within ±1 standard deviation of observations [*Doherty et al.*, 2005]. Figure 1 compares observed and modeled TCO (surface to 200 hPa) in the tropics, averaged over the 3 years 1999–2001. Data are satellite measurements from the Global Ozone Monitoring Experiment (GOME) instrument (http://www.temis.nl [*Valks et al.*, 2003]); model results are from our control run, described below. Where there is missing data in the observations, we have excluded model data for these months, so the comparison is not biased by sampling. Figure 1 shows that STOCHEM broadly simulates the major features of tropical TCO with close to the correct magnitudes. In particular, the low values over the Pacific warm pool region are well simulated, although the model has slightly lower values and the region is a little more extensive than observed. There are some discrepancies between the model

and GOME at around 20°N and 20°S, these are probably influenced by small differences in the simulated position of the subtropical jets, and hence the exact height and latitude of the tropopause in these regions. There are also differences over continental Africa and S. America, where the model tends to predict higher ozone than observed (in contrast to underestimates in HadAM3-STOCHEM compared to ozonesonde data as described above). These are probably related to the treatment and chemical processing of biomass burning emissions in the model.

2.2. Experiments

2.2.1. Present Day (1980–2002)

[11] Two "present-day" simulations were performed with HadAM3-STOCHEM. Both simulations use observed sea-surface temperatures (SSTs) as driving boundary conditions for HadAM3 for the period 1980–2002. Thus realistic SST changes associated with ENSO events have been included in HadAM3. In response to ENSO-related SST changes, HadAM3 simulates an atmospheric response: changes in the Walker circulation, precipitation, tropospheric humidity and air temperature. Trace gas anthropogenic and natural emissions evolve as prescribed by the SRES A2 scenario for the 1990s [*Nakićenović et al.*, 2000].

[12] In the first simulation ("control"), biomass burning emissions exhibit seasonality but are annually invariant. Global totals for biomass burning emissions for different species are based on *Prather et al.* [2001]. Spatial and seasonal distributions of these emissions are taken from *Cooke and Wilson* [1996] and are based on country estimates of area burnt. This simulation enables us to estimate the meteorological impact of ENSO.

[13] The second simulation ("varying biomass") uses different biomass burning emissions, but otherwise the same model setup and anthropogenic/other natural emissions as used in the control simulation. We used the *Duncan et al.* [2003] biomass burning emissions data set for 1979–1999 to incorporate interannual variability into our biomass burning data set. This data set uses an annual-mean inventory [*Yevich and Logan*, 2003] and seasonal emissions based on AVHRR and ATSR fire-count data. The interannual variability in the *Duncan et al.* [2003] data set was derived from the TOMS Aerosol Index (AI) product. *Duncan et al.* [2003] found the TOMS AI to be a reliable proxy of biomass burning for some world regions, and annual regional indices were constructed, for the following tropical regions: Indonesia, Brazil, Central America and Mexico and Southeast Asia. We applied these regional indices (courtesy of B. Duncan) to our existing seasonal biomass burning data set as used in the control simulation. For our experiment, we chose to retain the seasonality based on *Cooke and Wilson* [1996] because of the finer spatial detail ($5 \times 5^\circ$ grid cells compared to 4 tropical regions). There are several possible deficiencies in our data set: (1) We are combining two different proxies of biomass burning: seasonal black carbon emissions and annual TOMS AI; (2) we cannot distinguish any unusual single months of biomass burning since the seasonality is based on an annual average; (3) the seasonality is based on the mid-1980s; any shifts in seasonality between the 1980s and 1990s will therefore not be included; and (4) there is no interannual variability over Africa as the TOMS AI index was found to be an unreliable indicator of biomass burning due to contamination with desert dust and smoke.

2.2.2. Future

[14] We analyzed two further integrations performed with the coupled atmosphere-ocean GCM HadCM3 coupled to STOCHEM for 1990–2100, described by *Johnson et al.* [2002]. In one simulation ("climate change") greenhouse gases in the climate model evolve according to the SRES A2 scenario and in the other simulation ("control") they are held constant at their preindustrial values. In both simulations the SRES A2 scenario is used for trace gas anthropogenic emissions in STOCHEM. Natural emissions including lightning and biogenic isoprene (see section 2.1) are held constant (see *Stevenson et al.* [2000] and *Johnson et al.* [2002] for further details).

2.3. ENSO From Empirical Orthogonal Function (EOF) Analysis

[15] EOF analysis was performed to determine the leading mode of tropical variability on interannual timescales from detrended anomalies. The EOF spatial patterns (termed EOF1, etc.) and corresponding principal component time series (termed PC1, etc.) are then examined in relation to the widely used ENSO predictor, the Niño 3 index (average SST anomalies over 5°N–5°S, 150°E–90°W) for the first three EOF modes, to assess whether the leading mode of interannual variability represents ENSO. ENSO is always clearly depicted in EOF1 (unless otherwise discussed). In all our analyses, the *North et al.* [1982] rule is employed to ensure that EOF1 is well separated from higher EOF modes. EOF analysis was also used by *Peters et al.* [2001] to identify an ENSO-related tropospheric ozone signal in their chemistry transport model. EOF1 is scaled such that it is a unit vector (the sum of all squared values is equal to one) and the corresponding time series PC1 is scaled so as to equal the dot product of the EOF pattern and the data field at each time point. The original data can be recovered by multiplying each EOF pattern by its PC time series and summing over all EOFs [*Osborn*, 2004]. We multiplied EOF1 patterns by the standard deviation of the PC1 patterns to produce physical magnitudes of change for a "typical" (+1 standard deviation) El Niño or a "strong" La Niña (−1 standard deviation, i.e., inverse and weaker magnitudes than El Niño) event. Similarly, we scaled EOF1 patterns by the average PC1 value of the 1997/1998 and 1982/1983 El Niño events to obtain magnitudes of change for a strong El Niño event. Another method commonly used to construct a "typical" change map (i.e., a 1 standard deviation model El Niño event) is by regression of the normalized PC1 onto the original data anomalies [e.g., *Collins*, 2005]. We find a similar result using both methods and the former method is employed here.

3. Meteorological Impact of Present-Day ENSO

3.1. Changes in Meteorology

[16] Elevated SSTs during El Niño are accompanied by an eastward shift in the large-scale Walker circulation. This results in enhanced convection in the central and east tropical Pacific and reduced convection over Indonesia and the west Pacific, as shown in Figure 2a which depicts composites of El Niño–Normal (5 El Niño years between

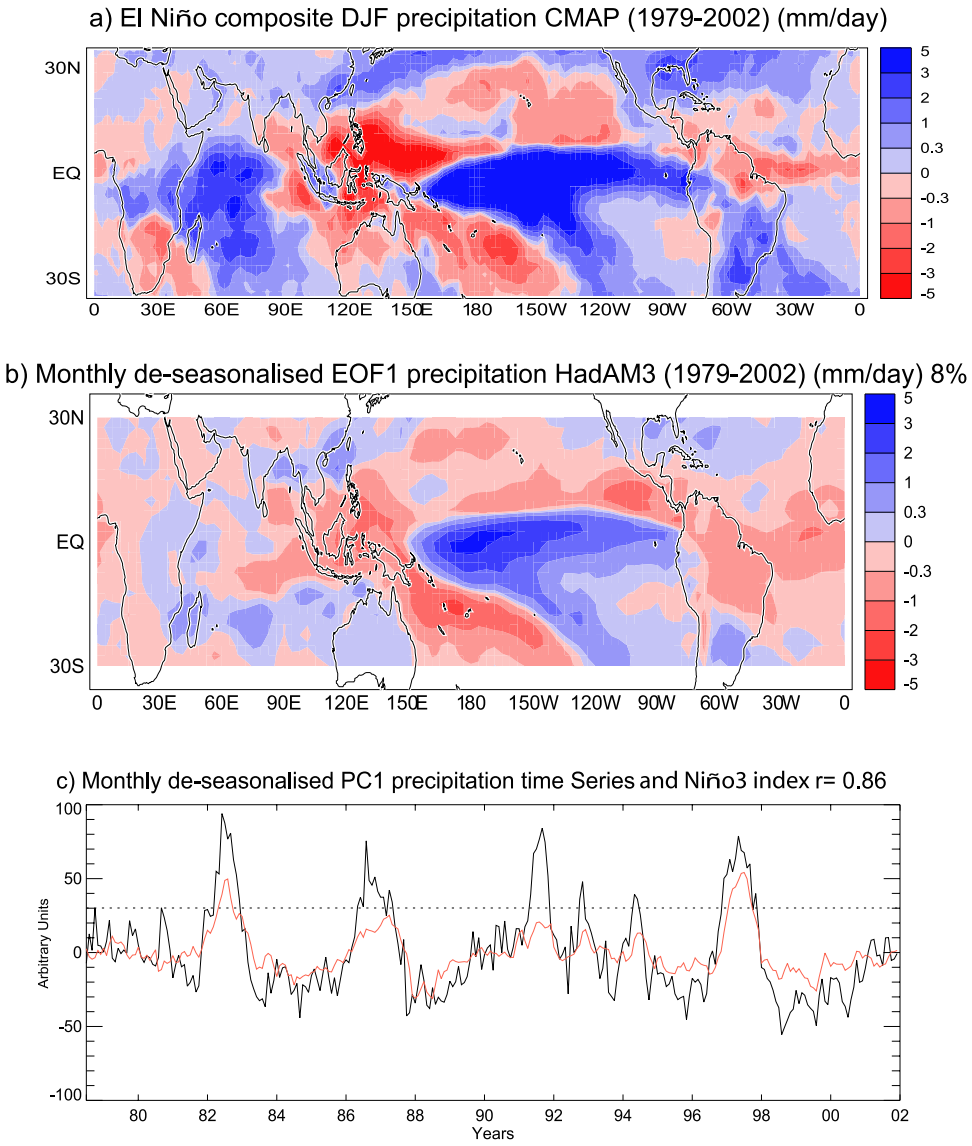

Figure 2. (a) El Niño minus normal composite of DJF precipitation from the CMAP data set for 5 El Niño years between 1980 and 2003. (b) Monthly deseasonalized EOF1 precipitation coefficients (scaled by +1 standard deviation of the PC1 time series) 1979–2002 (mm/day). Variance explained by EOF1 is 8%. (c) Corresponding PC1 precipitation time series (black) and scaled Niño 3 index (red) (correlation coefficient r = 0.86). +1 standard deviation of the PC1 time series is indicated by dotted line.

1980 and 2002) constructed from the CMAP observational data set [*Xie and Arkin*, 1996]. The first EOF of monthly deseasonalized precipitation from HadAM3 reproduces this ENSO pattern (Figure 2b, although weaker), and the PC1 time series, as expected, correlates closely with the Niño 3 index (r = 0.86) calculated from HadAM3 SSTs (Figure 2c). Since strong El Niño events (see section 2.3) have higher SST anomalies than strong La Niña events, Figure 2b depicts the change in precipitation for a "typical" El Niño (a +1 standard deviation change (section 2.3) corresponding to an El Niño of similar magnitude to that of 1994, or if the scale is reversed a strong "La Niña" similar to 1988). Unlike Niño 3 SST anomalies, which show 1997 as the strongest El Niño year, years 1982 and 1997 display similar changes in precipitation magnitude associated with El Niño (Figure 2c). Observed and modeled ENSO are tied to the annual cycle. An event usually commences in late spring to early summer and peaks typically in December/January.

[17] Figure 3 displays EOF1 updraught fluxes, with large-scale flow patterns for December 1997 (peak El Niño month) minus December 1996 (normal month) overlaid for the region 2.5°N to 7.5°S. Here EOF1 patterns are calculated separately for each model atmospheric layer for October-January (peak period) averages and then latitudinally averaged. All other vertical distributions discussed in section 3 have been calculated in the same way. The changes in precipitation (Figure 2) are generally reflected in the changed convection patterns throughout the troposphere (Figure 3). The weakening of the trade winds and a shift in the Walker circulation during El Niño result in downward motion in the western Pacific and Indonesian region and upward motion in the central Pacific (Figure 3).

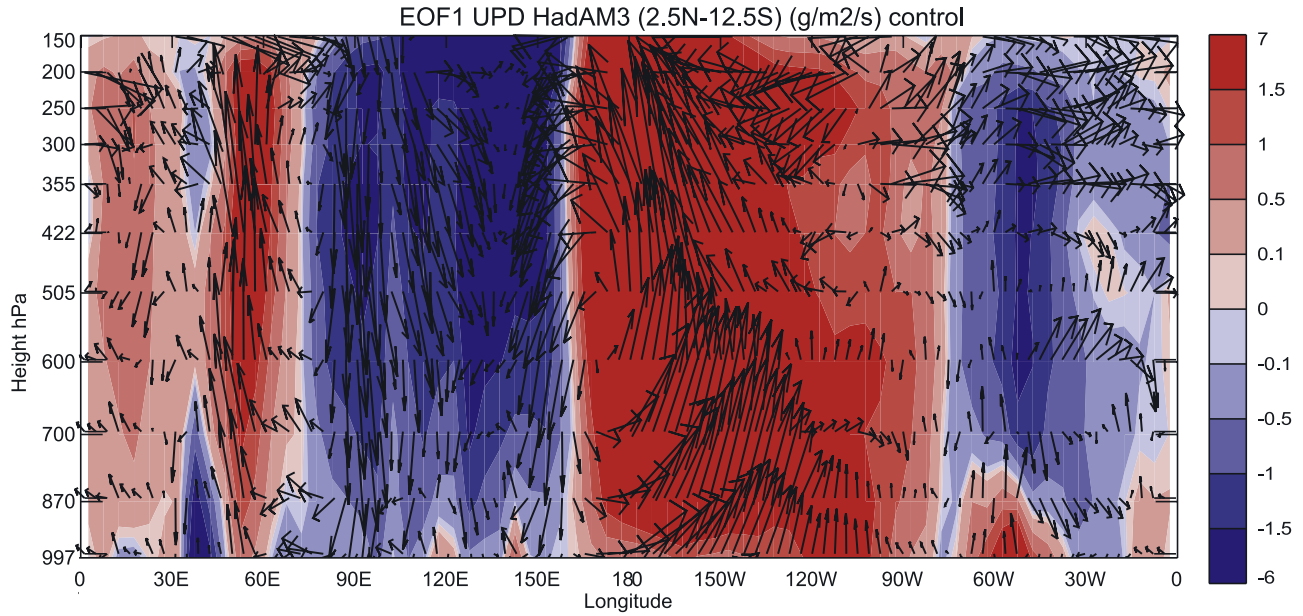

Figure 3. Shading showing the October-January "seasonal" average EOF1 convective updraught mass fluxes for each vertical level averaged over 2.5°N–7.5°S (scaled by +1 standard deviation of the PC1 time series) (g m^{-2} s^{-1}). Wind vector of zonal and vertical velocity (scaled) December 1997 (El Niño) to 1996 (normal) overlaid.

Also HadAM3 simulates enhanced upward motion in the Indian Ocean and strengthened westerly advection over the Atlantic in the UT. Specific humidity changes are similar to those depicted by *Sudo and Takahashi* [2001] and generally reflect the precipitation changes (not shown). Changes are largest in the MT and do not extend into the UT (not shown). Air temperatures (not shown) increase almost everywhere especially in the column above the Niño 3 region, the region of strongest updraught increases.

3.2. Changes in TCO and Column-Average NO_x

[18] The meteorological changes during ENSO result in a TCO pattern in HadAM3-STOCHEM that resembles an asymmetric dipole centered on the date line, as found in previous studies (section 1). The change in TCO for a "typical" and a "strong" (e.g., 1982/1983, 1997/1998) El Niño are depicted in Figures 4a and 4c respectively. Figure 4d displays a El Niño composite for DJF of 1982/1983 and 1997/1998 for comparison with Figures 4a and 4c. As expected, the results are qualitatively similar. PC1 TCO correlates well with the Niño 3 index (r = 0.63) (Figure 4b). EOF1 monthly deseasonalized TCO is reduced over the east and central Pacific and enhanced over the west Pacific/Indonesian region (Figure 4a). The region of TCO sensitivity to ENSO is more extensive than the region of precipitation sensitivity (Figures 2b and 4a). TCO decreases in the east Pacific extend eastward across South America. Likewise, TCO increases in the west Pacific extend across the Indian Ocean and into Africa.

[19] Over the central and east Pacific TCO decreases by 1–3 DU in peak months for "typical" El Niño events, (these are increases of similar magnitude for strong La Niña events) (Figure 4a), and by 4–10 DU in peak months during strong (1982/1983, 1997/1998) El Niño events (Figure 4c). Similarly, over the west Pacific, Indonesia and the Indian Ocean TCO increases by 0–2 DU for peak months during "typical" El Niño events (or decreases by a similar amount for strong La Niña events) and increases by 0–6 DU for strong El Niño events. In terms of annual-average changes (July(0)-June(+1) year) TCO decreases by 1–2 DU (2–6 DU) in the central and east Pacific during typical (strong) El Niño years, and increases by 0–1 DU (0–2 DU) in the west Pacific/Indonesia (not shown).

[20] In the central and east Pacific, the simulated TCO anomaly magnitudes for a strong El Niño event are in good agreement with studies of TCO changes during October 1997 [*Chandra et al.*, 1998; *Sudo and Takahashi*, 2001; *Chandra et al.*, 2002]. They are higher than those of *Ziemke and Chandra* [2003] for a peak event. Anomalies for a "typical" El Niño event also agree with previous studies [*Ziemke and Chandra*, 1999, 2003; *Peters et al.*, 2001]. However, there are some differences in spatial patterns. In particular, the TCO minimum is displaced further eastward in our study such that negative TCO anomalies extend over South America. We believe that this extension of negative TCO anomalies is mainly related to changes in lightning NO_x emissions (see below) which in reality may be offset by changes in biomass burning emissions.

[21] However, changes in the west Pacific for a peak El Niño event are underestimated in our study compared to previous studies that excluded the effects of variable biomass burning [*Sudo and Takahashi*, 2001; *Chandra et al.*, 2002]. Changes during a normal El Niño event (excluding biomass burning) are slightly less than those calculated by *Peters et al.* [2001]. In terms of spatial patterns, the location of the TCO maxima agrees with *Peters et al.* [2001], who also use EOF1 analysis to characterize ENSO, but is displaced further northeast than in the other aforementioned studies. However, these previous studies have examined

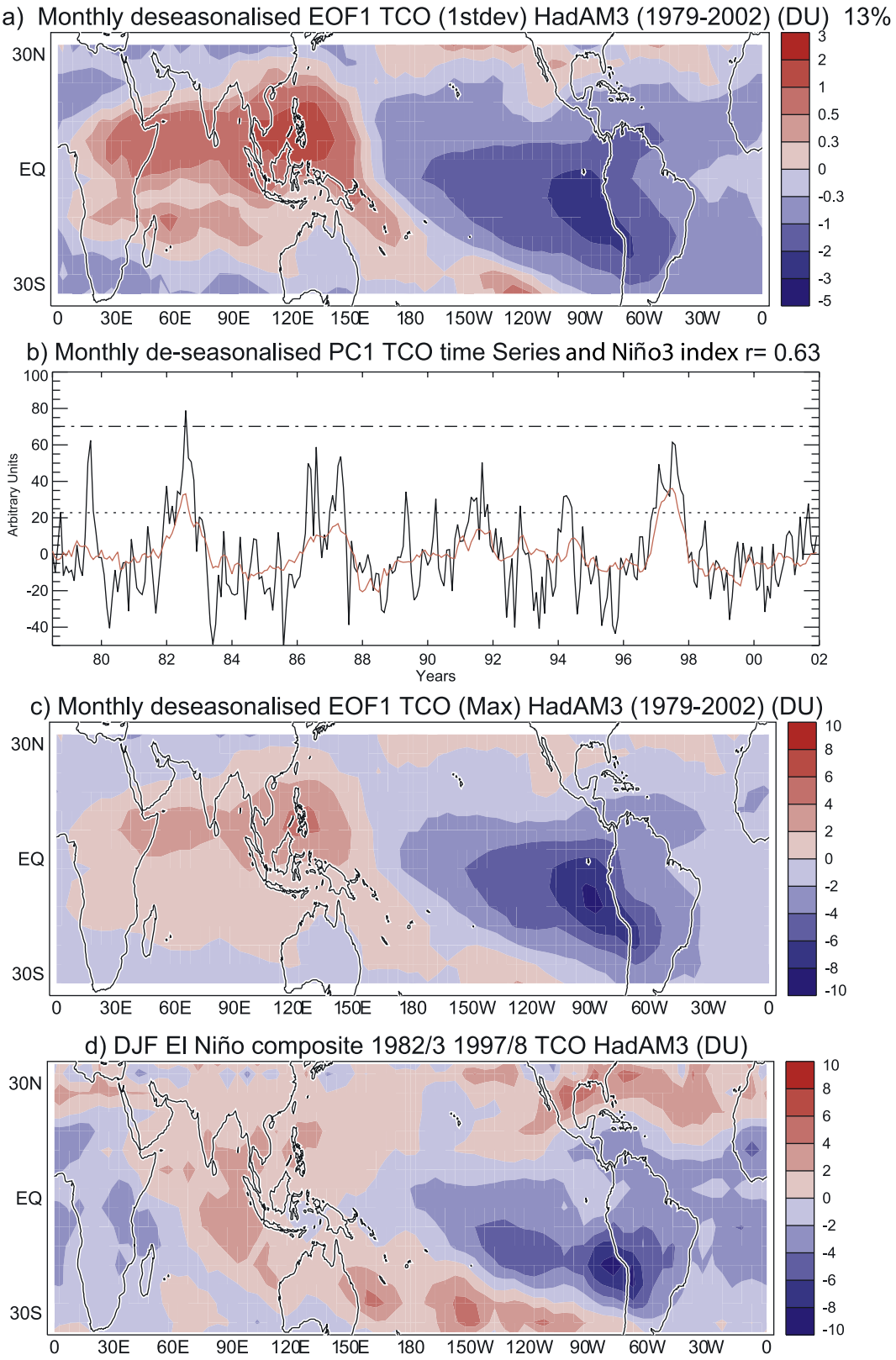

Figure 4. Monthly deseasonalized (a) EOF1 TCO coefficients (scaled by +1 standard deviation of the PC1 time series) 1979–2002 (DU), where variance explained by EOF1 is 13%; (b) PC1 TCO time series (black) and scaled Niño 3 index (red) (r = 0.63), with +1 standard deviation indicated by the dotted line and the mean of 1982/1983 and 1997/1998 peak months termed "MAX value" indicated by dot-dashed line; (c) EOF1 TCO coefficients scaled by MAX value (see above) of the PC1 time series; and (d) El Niño minus normal composite for years 1982/1983 and 1997/1998 of DJF TCO (DU).

ENSO-induced TCO changes between October 1997, a month of unprecedented enhanced TCO from biomass burning, and October 1996 (a normal year). Between October 1997 and January 1998, our model simulates a strengthening and eastward shift of negative TCO anomalies in the central and east Pacific, and a southwest to northeast shift of positive TCO anomalies over Indonesia (not shown). Similar patterns of TCO anomaly shifts occur in our model in 1982 (not shown). The EOF1 pattern picks out the dominant spatial and temporal pattern of variability in the 1980–2002 period. Since the meteorological impact of ENSO peaks in December/January, we find the EOF1 pattern is more representative of the December/January rather than the October TCO changes. Examining October 1997 relative to 1996 we find that spatial patterns of simulated TCO differences are similar to those of the previous studies discussed above, however the magnitude of change is still underestimated.

[22] Monthly deseasonalized EOF1 column-average NO_x decreases over Indonesia and South America (5–10 ppt for ''typical'' El Niño conditions; Figure 5a) are associated with suppressed lightning NO_x emissions over these land regions (Figure 5c; see also Figure 7b). As mentioned above, the reduction in the lightning NO_x source offsets potential ozone increases due to suppressed convection over Brazil. PC1 NO_x correlates with the Niño 3 index at r = 0.2 (but r = 0.7 for a ''seasonal'' October-January average, see below) (Figure 5b). PC1 for lightning NO_x emissions has a stronger relationship with ENSO (r = 0.47; Figure 5d). Increased convection over the Andes and East Africa produce lightning NO_x increases. Increased convection over the sea also produces lightning NO_x increases over the Pacific and Indian oceans but these are much smaller compared to changes over land (Figure 5c). The effect of changes in lightning over the oceans could be too small, as the *Price et al.* [1997] lightning NO_x scheme is thought to underestimate oceanic lightning [*Doherty et al.*, 2005; *Labrador et al.*, 2005].

3.3. Vertical Trace-Gas Changes

[23] Figure 6 displays October-January average EOF1 ozone changes latitudinally averaged between 2.5°N to 7.5°S through the atmosphere, calculated as described in section 3.1. With increased convection and upward motion in the central and east Pacific during El Niño, low ozone content surface air displaces UT air with higher ozone concentrations. This results in ozone decreases throughout the tropospheric column (Figure 6b). As discussed above, the extension of these negative anomalies over South America is primarily related to decreased NO_x from lightning (Figures 5c and 7b); enhanced advection from the east Pacific in the UT may also make a small contribution (Figure 3). MT/UT O_3 decreases are between 1–5 ppb (~5–20%) for a ''typical'' El Niño (Figure 6b). Corresponding decreases for a strong El Niño event are 2–20 ppb (~10–100%) (Figure 6c), which are similar to ozone changes simulated for October 1997/1998 by *Zeng and Pyle* [2005] and *Sudo and Takahashi* [2001]. Suppressed convection over the west Pacific/Indonesia and along the South Pacific Convergence Zone (SPCZ) leads to increased MT/UT ozone between 0.5 and 3 ppb (4–10%) for a typical and between 2 and 15 ppb (8–50%) for a strong El Niño event (Figure 6). This change is considerably lower (except in the upper UT) than simulated in the aforementioned studies above.

[24] Positive UT ozone anomalies extending west across the Indian Ocean are a feature of this and previous studies. Enhanced downward motion (Figure 3) above the Indian Ocean may be important in bringing higher amounts of ozone-rich air of stratospheric origin into the UT, as well as lowering tropopause height. However, the simulated increase in tropopause pressure over the Indonesian region during strong El Niño events is rather small (<20 hPa). Positive UT anomalies in the Indian Ocean merge with positive UT anomalies over East Africa. The latter coincides with a LT ozone decrease. Enhanced convection and large-scale uplift over polluted biomass burning regions of eastern Africa (where surface ozone >60 ppb, Figure 6a) will have a different effect on the vertical ozone distribution compared to enhanced convection over the remote Pacific where surface ozone concentrations are low (Figure 6a). Lifting of polluted ozone-rich surface air leads to reduced LT and enhanced UT ozone around 30°E (Figure 6b).

[25] We have discussed El Niño–induced changes in large-scale and convective transport and how these modulate tropospheric ozone. El Niño–induced changes in chemistry, through changes in temperature, water vapor and climate-dependent emissions, also contribute to the ozone changes displayed in Figure 6. Ozone net chemical production decreases in the MT and UT over South America (Figure 7a). Changes in UT net chemical production appear to be mainly associated with changes in NO_x (Figure 7b). The lower part of Figure 7b (also upper parts of Figures 7c and 7d) is masked off as the EOF analyses on these levels do not show a significant ENSO-related signal. Shifting convection away from land regions results in UT NO_x decreases over Indonesia (1–10 ppt) and South America (10–55 ppt) (Figure 7b). Surprisingly, wet deposition of HNO_3 does not appear to be significantly affected by El Niño–related precipitation changes. However, HNO_3 concentrations (not shown) are influenced by El Niño–related NO_x and HO_x changes; these are discussed below. El Niño–induced changes in NO_x are markedly different to those shown by *Sudo and Takahashi* [2001]. The changes in NO_x distribution in our study are dominated by changes in lightning NO_x, while the NO_x vertical distributions by *Sudo and Takahashi* [2001] (although they do show a reduction in UT NO_x over Indonesia) depict much more extensive changes that are similar to their ozone changes.

[26] Changes in LT and MT net ozone chemical production (Figure 7c) are the result of the residual changes in ozone chemical production and loss. Absolute production and loss terms are strongly driven by HO_x changes (Figure 7c); this is less clear in the net field shown in Figure 7a. These HO_x changes are partly associated with humidity and precipitation (wet removal) changes (not shown) and are also partly related to enhanced isoprene over land regions (Figure 7d), Isoprene emissions over land regions are enhanced (~5–10%) as a result of El Niño–induced temperature increases.

3.4. Importance of ENSO in Relation to Global Ozone Budget

[27] The ENSO signal influences tropical and global burdens of chemical species and global chemical fluxes.

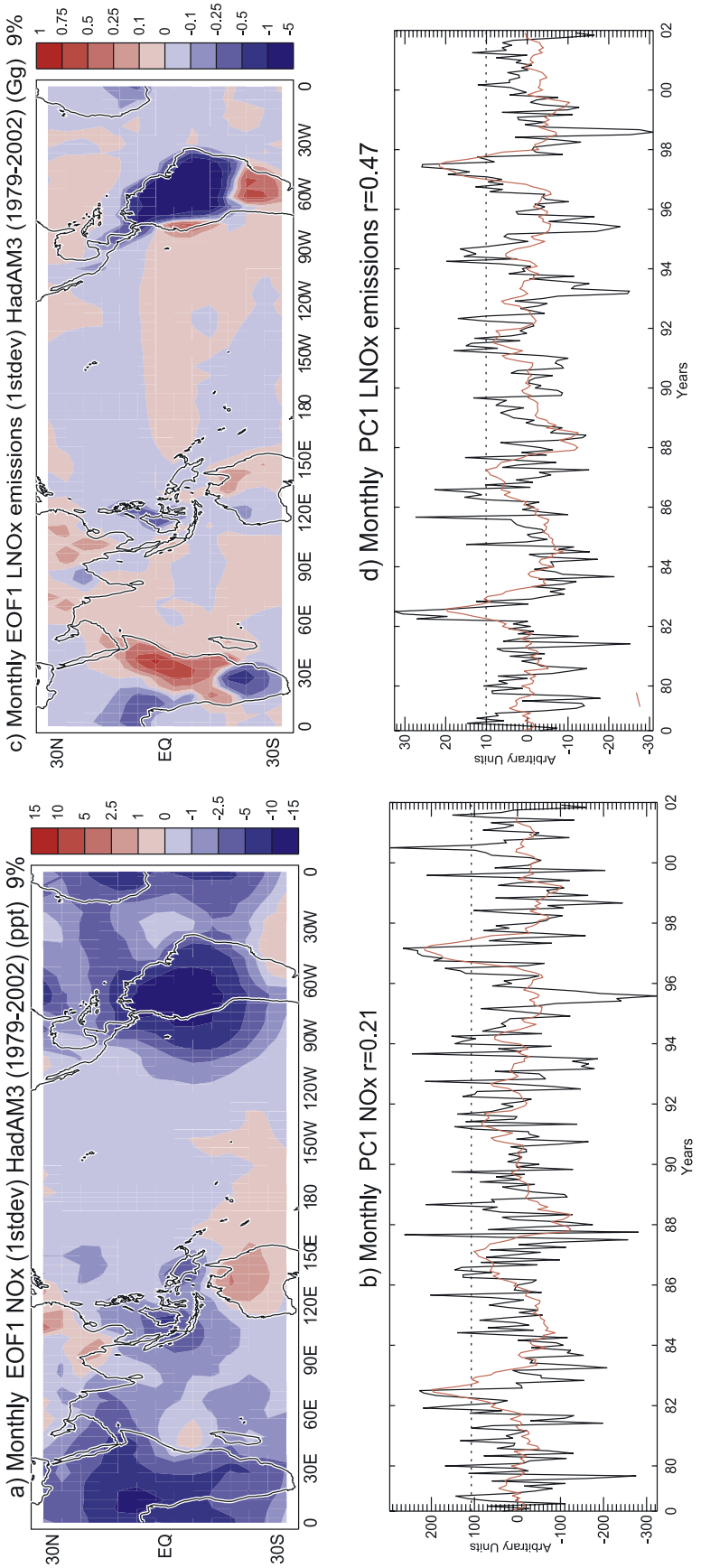

Figure 5. Monthly deseasonalized (a) EOF1 column-average NO_x coefficients (scaled by +1 standard deviation of the PC1 time series) 1979–2002 (ppt), where variance explained by EOF1 is 9%, and (b) PC1 column-average NO_x time series (black) and scaled and Niño 3 index (red) (r = 0.21), with +1 standard deviation of the PC1 time series indicated by dotted line. (c and d) As for Figures 5a and 5b but for lightning NOx emissions (Tg N/yr). Variance explained by EOF1 in Figure 5c is 9%, and in Figure 5d, r = 0.47.

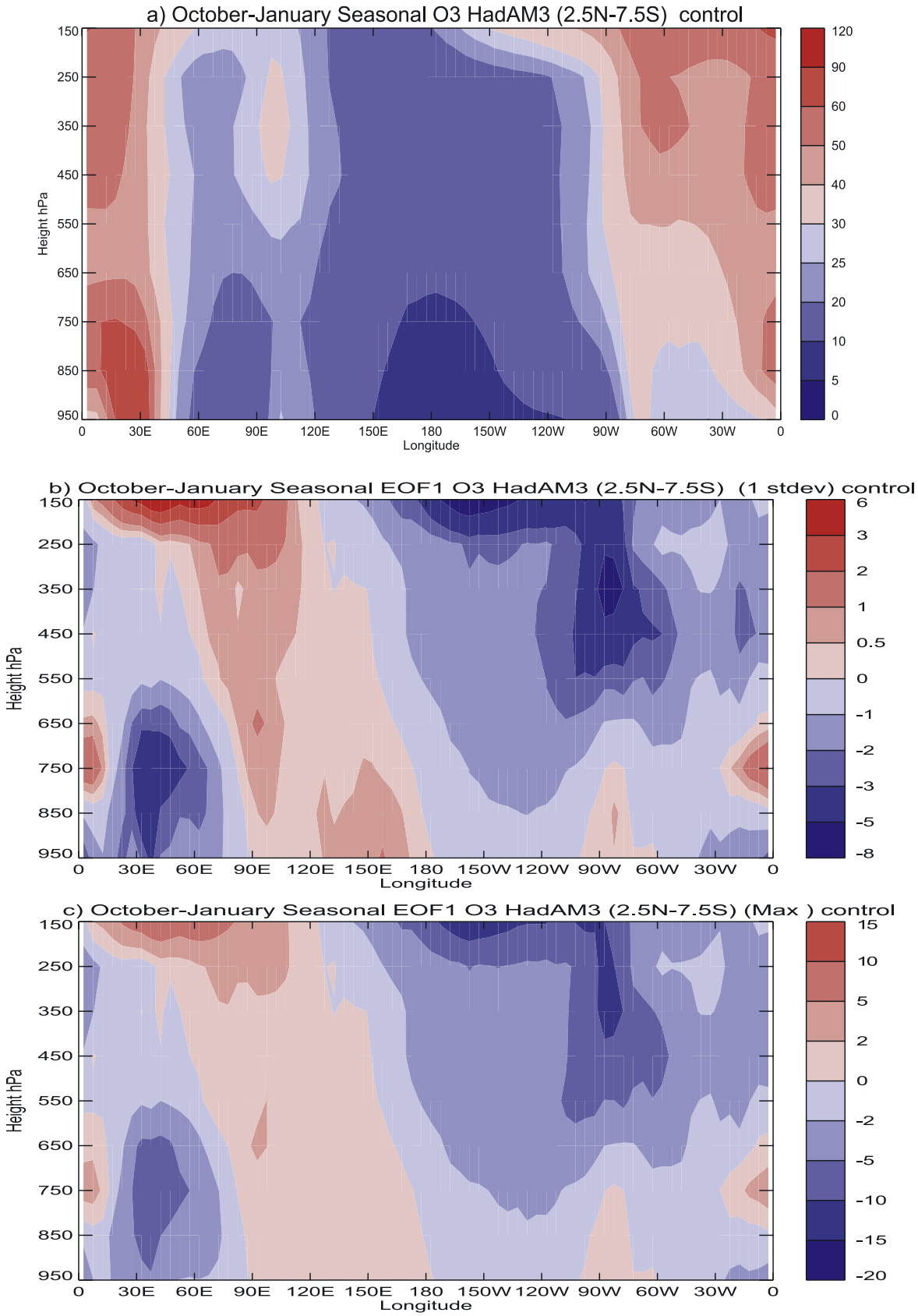

Figure 6. October–January "seasonal" average (a) tropospheric ozone averaged between 2.5° N–7.5°S (ppb), (b) EOF1 tropospheric ozone (scaled by +1 standard deviation of the PC1 time series) for each vertical model level averaged between 2.5° N–7.5°S (ppb), and (c) as in Figure 6b but scaled by MAX value (see Figure 4) of the PC1 time series.

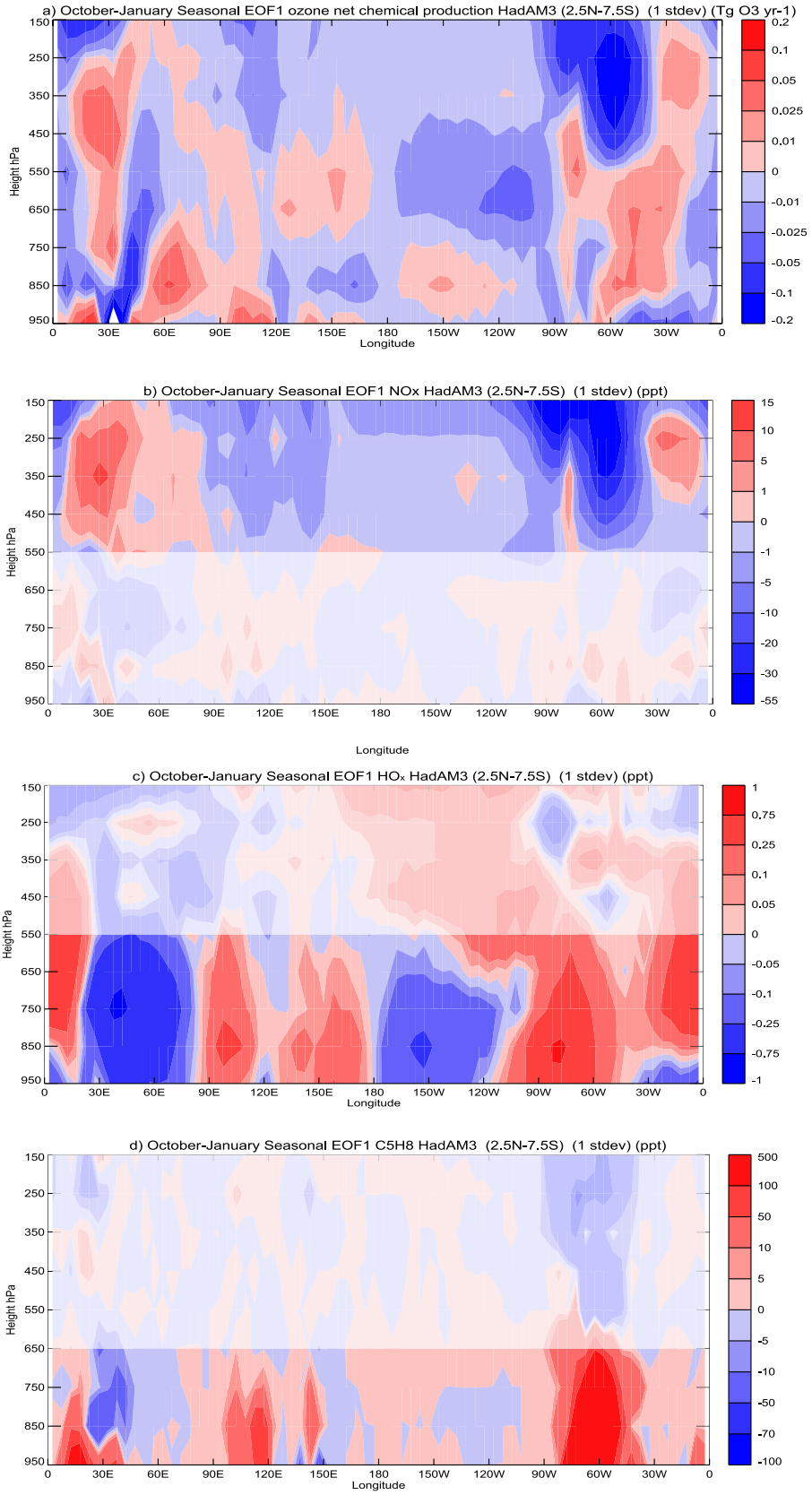

Figure 7. October–January "seasonal" average EOF1 (a) net ozone chemical production (scaled by +1 standard deviation of the PC1 time series) for each vertical model level then averaged between 2.5°N–7.5°S (Tg O_3 yr^{-1}), (b) as in Figure 7a but for NO_x (ppt), (c) for HO_2 (ppt), and (d) for isoprene (ppt). Whitened regions in Figures 7b–7d are where no strong ENSO signal was found in the EOF analyses for that model vertical level; that is, the PC1 times series exhibits no relationship with the Niño 3 index.

Table 1. Correlation Coefficients Between Global and Tropical Burdens and the Niño 3 Index, and for the Niño 3 Index Leading by 6 Months[a]

Correlation Coefficient r Between Burden/Flux and Niño 3 Index	Global Burden	Global Burden (Niño 3 Index +6 Months)	Tropical Burden	Tropical Burden (Niño 3 Index +6 Months)	Global Burden El Niño (1997)/La Niña (1988) for Species With r > 0.74
O_3	−0.55	−0.78	−0.86	−0.59	245/254 (+6) TgO_3
NO_x	−0.64	0.07	−0.70	−0.03	0.146/0.155 (0) Tg N
C_5H_8	0.54	0.88	0.49	0.87	0.123/0.113 Tg (+6)
OH	−0.75	−0.05	−0.77	−0.09	197/207 (0) Mg OH
HO_2	0.62	0.89	0.68	0.90	11220/11026 Mg HO_2 (+6)
O_3 production	−0.16	0.61	−0.26	0.58	
O_3 loss	0.03	0.59	0.20	0.76	
O_3 NCP	−0.47	0.22	−0.74	−0.06	
O_3 dry deposition	−0.56	−0.63	−0.61	−0.64	
O_3 strat. influx	0.24	−0.44	0.64	−0.08	
Surface air temperature	0.13	0.31	0.64	0.75	5.2/5.0°C (+6)
Surface humidity	0.40	0.71	0.52	0.75	38.0/37.2 g/Kg (+6)

[a]The final column shows the global burdens (and temperatures/humidities) for the 1997 El Niño and 1998 La Niña years to illustrate the magnitude of variability. r > 0.51 (0.74) for significance at 0.01 (0.001) level. (0) = El Niño/La Niña year (+6) = El Niño/La Niña year +6 months.

Table 1 displays the correlation coefficient between the Niño 3 index and annual detrended burdens and fluxes globally and for the tropics. Also displayed are the same correlations but with the Niño 3 index leading the chemical species/flux by 6 months. The relationship between the monthly Niño 3 index and the listed chemical species burdens is unsurprisingly highest in the tropics for a zero month lag for ozone, NO_x, CO and OH, but for HO_2 and isoprene is higher with a 6-month lag. Surface air temperature (averaged over the tropics) also shows a higher correlation for a 6-month lag (Table 1), as the atmospheric response to elevated SSTs in the Niño 3 region propagates throughout the tropics and globe. This suggests that ENSO-related temperature variability is the main source of tropical HO_2 variability through temperature-dependent variations in land-based isoprene emissions, while OH variability is driven predominantly by ENSO-related variability in NO_x. The final column in Table 1 gives values for global burden/fluxes for the peak El Niño (1997) and La Niña (1988) year in the 20-year period, if the correlation coefficient between the Niño 3 index and global burden/flux (0 or 6-month lag) is above 0.74 and significant at the 0.001 level (see Table 1).

[28] The relationship between Niño 3 index and the global ozone, HO_2 and isoprene burdens is however stronger with a 6 month lag between the ENSO signal and the global species response. This is not the case for the other species listed.

[29] The ozone production and destruction and dry deposition fluxes also have a stronger relationship with ENSO with a 6 month lag, both in the tropics and globally. This suggests that ENSO-driven variations in LT and surface climate (Table 1) control variations in ozone fluxes (which are largest at the surface). However, net ozone chemical production exhibits a higher correlation for a zero month lag. Stratospheric ozone influx changes from a positive correlation at zero month lag to a negative correlation at 6 month lag. *Zeng and Pyle* [2005] also found a negative correlation between the SOI (another index of ENSO) and STE (with STE lagged by 6 months), although their correlation was much higher (r = −0.6). They used the same climate model HadAM3 in their experiments, but coupled to a different chemistry model. Their chemistry model UM-CAM has a higher vertical lid, higher vertical resolution in the tropopause region, and includes some chemistry in the lower stratosphere, which may explain their higher model sensitivity of STE to ENSO.

4. Biomass Burning Impact of Present-Day ENSO

[30] Figure 8 depicts EOF1 ozone for a typical El Niño for the control and biomass burning simulations for the August to January season. We have chosen a different averaging period in order to encompass the biomass burning season over Indonesia, which peaks earlier (August/September) than peak ENSO months of elevated SSTs (December/January).

[31] There are two important points to note. As discussed above, annually varying biomass burning emissions were not available for Africa, thus the biomass burning emissions over Africa are the same as in the control simulation. Moreover, in our annually varying biomass burning emissions data set we use a seasonally invariant biomass burning data set scaled by yearly totals. This construction method was chosen in order to avoid spatial seasonal discontinuities between model grid cells which fall within and outside regions where annually varying biomass burning emissions were available. However, this approach of scaling each month by the same annual value, means that we will underestimate biomass burning emissions in their peak month/s. Comparing the monthly variability in our constructed data set with that of the TOMS monthly AI index (supplied by B. Duncan), we find we have underestimated biomass burning emissions over Indonesia by a factor of ∼2 during September/October 1997, the months with largest observed AI index. Using a seasonally invariant data set also means that Indonesia always has peak emissions in August/September and not in September/October in 1997 as observed.

[32] Figure 8 shows that the El Niño signal is slightly different in spatial structure and lower in magnitude than that obtained in Figure 4 from the monthly data, as a result of the longer averaging period. Increased biomass burning with El Niño augments the El Niño induced TCO change over Indonesia by 0.5–1 DU during a typical and by 1–2 DU during a strong El Niño. The direct contribution of TCO due to El Niño–enhanced biomass burning emissions is displayed in Figure 9 for El Niño years: 1982/1983, 1991/1992, and 1997/1998. TCO increases by

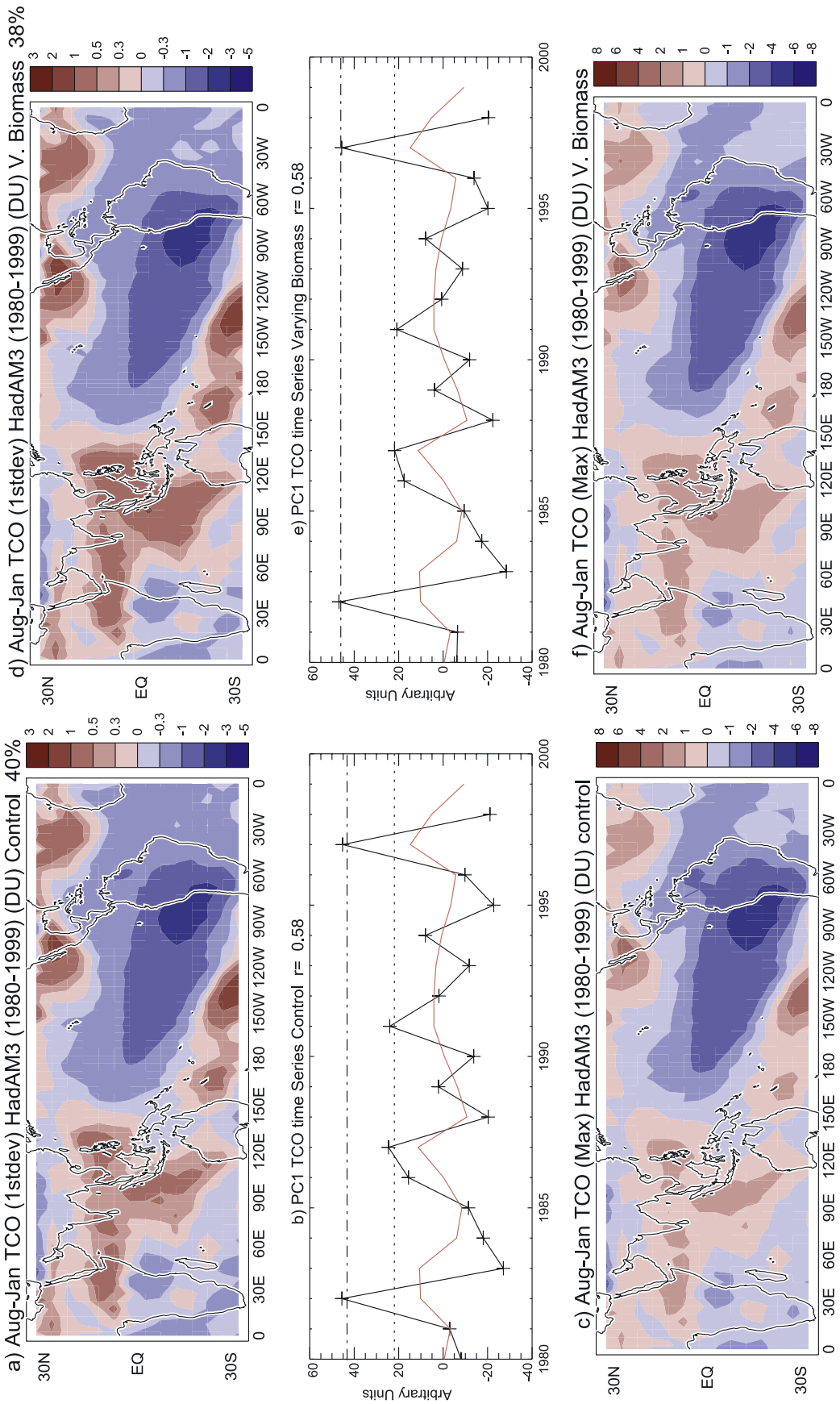

Figure 8. August–January "seasonal" average (a) EOF1 TCO coefficients (scaled by +1 standard deviation of the PC1 time series) 1979–2002 (DU), where variance explained by EOF1 is 40%; (b) PC1 TCO time series (black) and scaled Niño 3 index (red) (r = 0.58), with +1 standard deviation and MAX value (see Figure 4) indicated by dotted and dot-dashed lines; and (c) EOF1 TCO coefficients (scaled by MAX value of the PC1 time series) (DU), all for the control simulation. (d–f) As Figures 8a–8c but for the annually varying biomass burning emissions simulation (variance explained = 38%, r = 0.57).

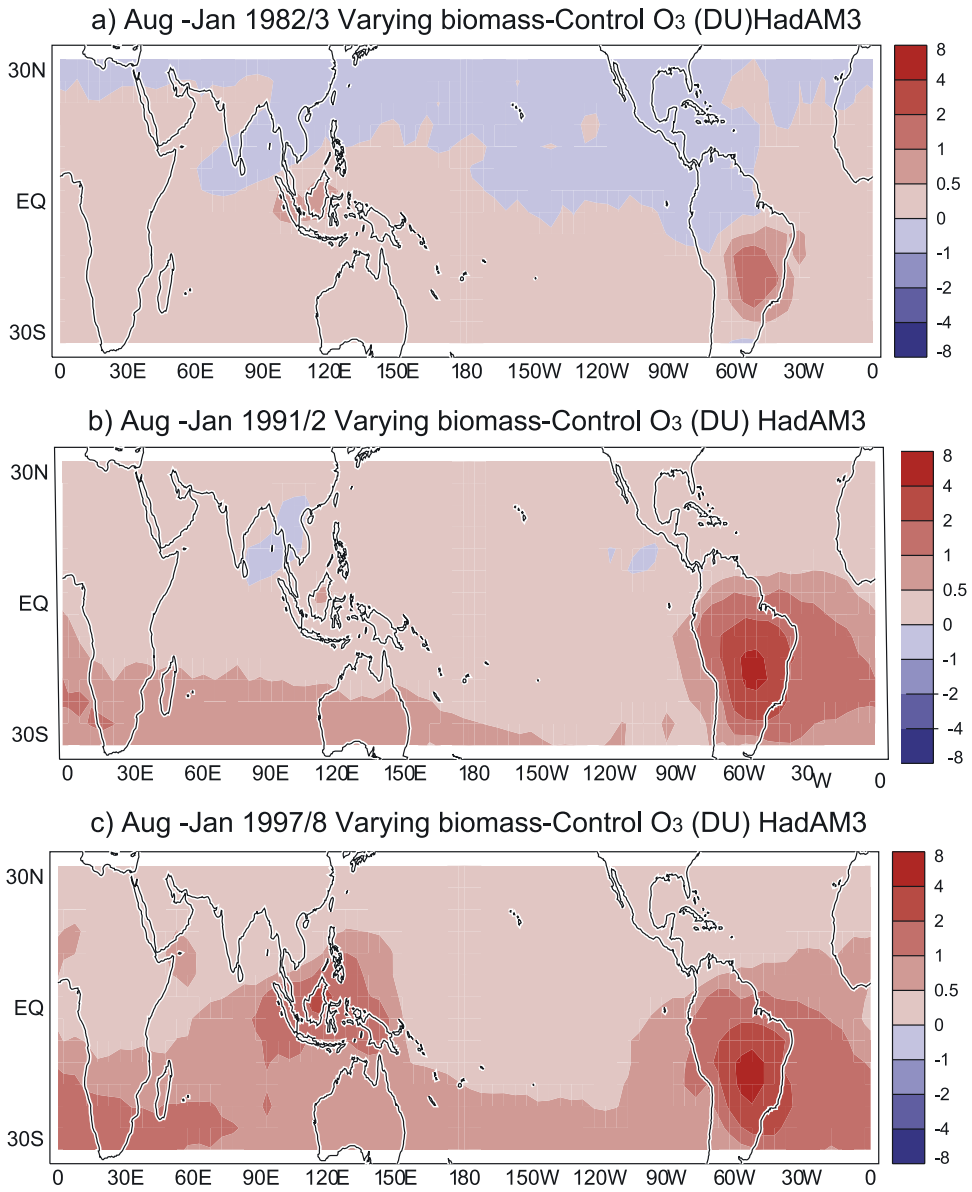

Figure 9. August–January "seasonal" average TCO from the annually varying biomass burning emissions simulation relative to results from the control simulation, for El Niño years: (a) 1982/1983, (b) 1991/1992 and (c) 1997/1998.

0–1 DU during August-January 1982/1983 and 1991/1992 and by 1–4 DU during August-January 1997/1998 over Indonesia and by 1–8 DU over Brazil. TCO increases are ~4 DU over Indonesia and ~8 DU over Brazil when only September/October 1997 is considered. This increase in TCO over Brazil negates the El Niño–induced ozone reduction over Brazil due to decreased lightning NO_x emissions (Figure 5c) between September and October. However, the enhanced biomass burning ceases before December/January when the SST anomalies peak. The EOF patterns appear to be dominated by the ozone changes during peak SST months, and therefore the enhanced ozone in the earlier months due to elevated biomass burning is not strongly represented. The increase in EOF1 ozone due to elevated biomass burning during El Niño is strongest in the LT, but there are slight MT/UT increases (not shown). This suggests that there is still some venting of the boundary layer over Indonesia during El Niño conditions.

[33] The September/October simulated TCO increases with elevated biomass burning during El Niño in 1997 over Indonesia are significantly less than the increases (~12 DU) simulated for October by *Chandra et al.* [2002]. However, the sensitivity experiment by *Chandra et al.* [2002] compared two simulations one with and one without biomass burning emissions, whereas our simulations compare differences between a biomass burning climatology and time series. Nevertheless, our simulated increases are much lower than observed TCO increases during September/October 1997.

5. Future ENSO

[34] In the HadCM3-STOCHEM simulation with the SRES A2 climate forcing scenario the global mean surface

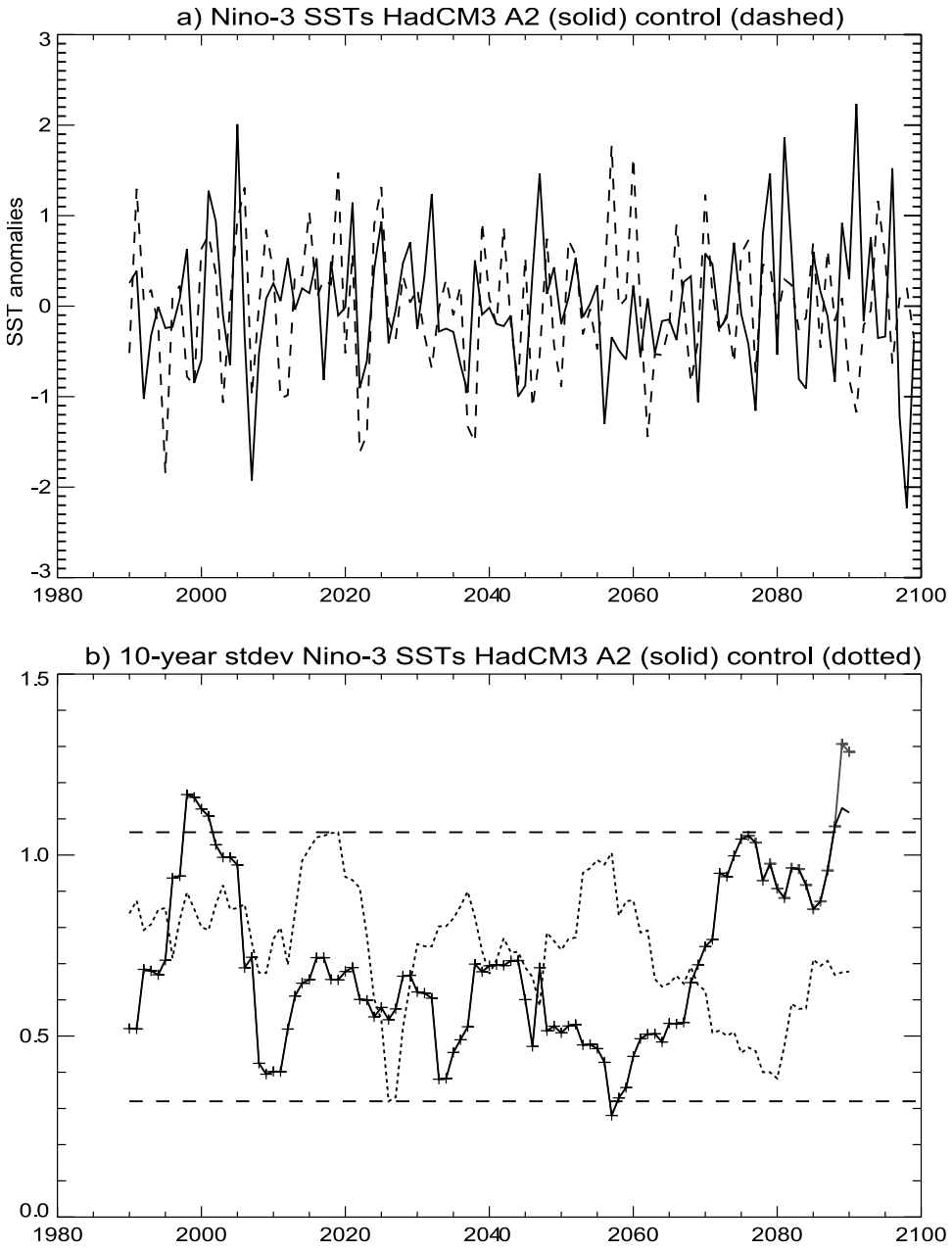

Figure 10. (a) Annual Niño 3 SST index for HadCM3 SRES A2 (solid) and control (dashed) simulations and (b) 10-year running mean standard deviation of annual Niño 3 SST index SRES A2 (solid) and control (dotted). Maximum and minimum values from the control simulation are depicted as dashed lines.

temperature increases by 3.6 K between 2000 and 2100. HadCM3 is one of several GCMs that suggest a possible mean future El Niño–like state in the tropical Pacific as discussed in section 1 [*Williams et al.*, 2001; *Cox et al.*, 2004]. Changes in temperature and precipitation between the 2090s and 1990s decades in this HadCM3 simulation (not shown) resemble those of Figure 4 by *Cox et al.* [2004], although the warming is slightly greater in our simulations that use the SRES A2 scenario, compared to the IS92a scenario used by *Cox et al.* [2004]. We calculated the trend in surface air temperature, precipitation and TCO over the 110-year period (1990–2100). For TCO we calculated the trend in the climate change minus the control simulation in order to separate the climate change signal in ozone from that relating to changing precursor emissions. The trend in temperature appears broadly El Niño–like, with increases above 3°C per century in the central and east Pacific and 2°–3°C per century in the west Pacific (not shown). Precipitation also has an increasing trend (2–5 mm/day per century) across the ITCZ in the central and east Pacific and a decreasing trend over Indonesia (1–3 mm/day per century). However, the trend in TCO is negative across the entire Pacific region and there is no evidence of an El Niño–like contrast between the trend in the east and west Pacific (not shown). Therefore future El Niño–like changes in temperature and precipitation in the tropical Pacific do

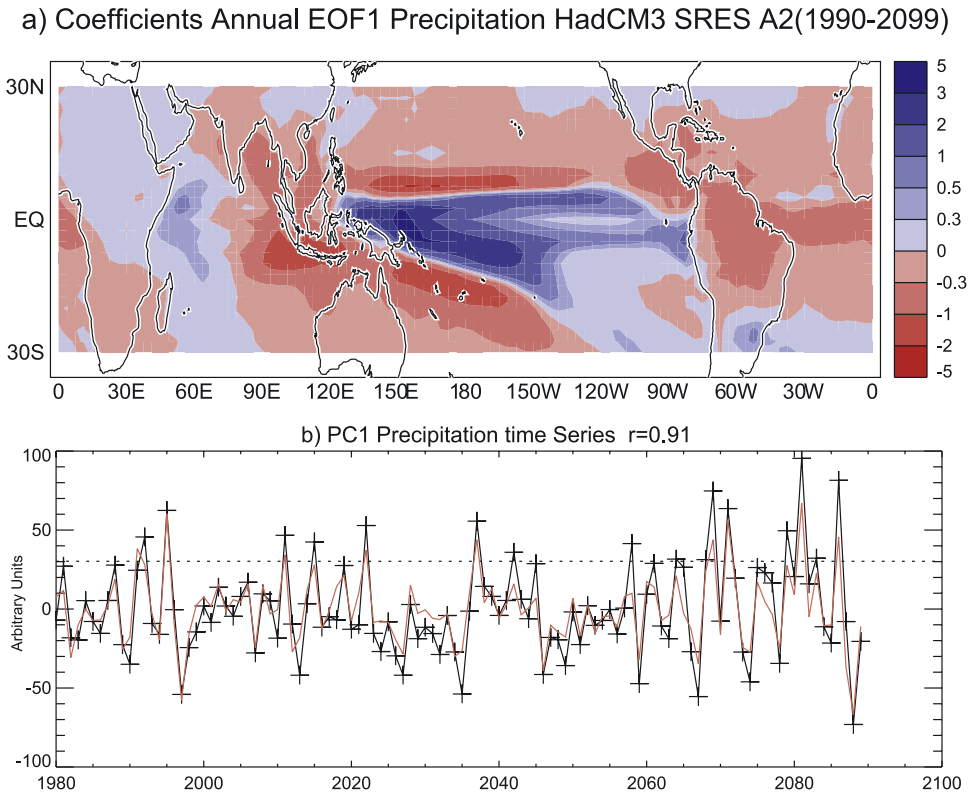

Figure 11. October–January "seasonal" average (a) EOF1 precipitation (scaled by +1 standard deviation of the PC1 time series) 1990–2099 (mm/day) and (b) PC1 precipitation time series (black) (+1 standard deviation depicted by dotted line) and Niño 3 index (red) (r = 0.91) for HadCM3 SRES A2 simulation.

not appear to be the dominant influence on TCO over the 100-year period. The negative TCO trend reflects enhanced ozone destruction resulting from higher humidities in a warmer climate. A water vapor feedback on tropical LT ozone under future climate is a robust feature of climate-chemistry model simulations [*Johnson et al.*, 2002; *Stevenson et al.*, 2006].

[35] Following *Collins* [2005] we also calculated the spatial pattern correlation coefficient between the 110-year trend and the EOF1 across the tropical Pacific for these three variables. The spatial pattern correlation did not exceed 0.3 for any of the three variables. Therefore, despite qualitatively similar spatial patterns in the 21st century trend and ENSO (as derived from EOF1 patterns) across the Pacific for temperature and precipitation, the areas of maximum change are not exactly colocated.

[36] Changes in ENSO variability have been examined by *Collins* [2000] in the HadCM2 and HadCM3 GCMs. In contrast to results from HadCM2 and a previous study by *Timmermann et al.* [1999], *Collins* [2000] found no change in ENSO SST variability in a HadCM3 simulation with quadrupled CO_2 concentrations. We examined ENSO variability between 1990 and 2100 in this HadCM3 SRES A2 simulation. On the basis of the results above we expected little change. The annual-average Niño 3 index for 1990–2100 is shown in Figure 10a for the increasing greenhouse gas SRES A2 scenario and for the control (i.e., with no greenhouse gas forcing) simulation. In the SRES A2 simulation we see that the SST variability increases in the last decades of the experiment, unlike in the control experiment. The time series of 10-year running mean Niño 3 interannual standard deviations (Figure 10b) shows an upward trend from 2070, but this only exceeds the maximum value of the standard deviation in the control simulation in the last few years. Removing the largest negative Niño 3 index value (in 2098) from the SRES A2 Niño 3 time series and recalculating the 10-year running standard deviation still yielded values that were marginally above the maximum standard deviation from the control simulation. Therefore (as found by *Collins* [2000]) there is little evidence of a robust increase in SST variability in the future period. However, this is not the case for precipitation. The first EOF of annual-average precipitation for the SRES A2 simulation is displayed in Figure 11. As with HadAM3-STOCHEM (Figure 2), the ENSO-like signature in precipitation is a robust feature in the HadCM3-STOCHEM simulation, and the PC1 time series correlates at r = 0.9 with the Niño 3 index. Unlike the Niño 3 index, the PC1 precipitation time series exhibits greater variability from the mid 2060s (Figure 11b). The ENSO pattern is also clear in EOF1 precipitation for the control simulation, but PC1 in this control simulation shows no obvious change in variability (not shown). EOF1 October-January average TCO for the SRES A2 simulation is depicted in Figure 12a. Again, the pattern of TCO change in HadCM3-STOCHEM is similar to that displayed by HadAM3-STOCHEM in Figure 4a. Note that in Figure 4 the EOF analysis is performed on monthly deseasonalized TCO while in Figure 12 the EOF

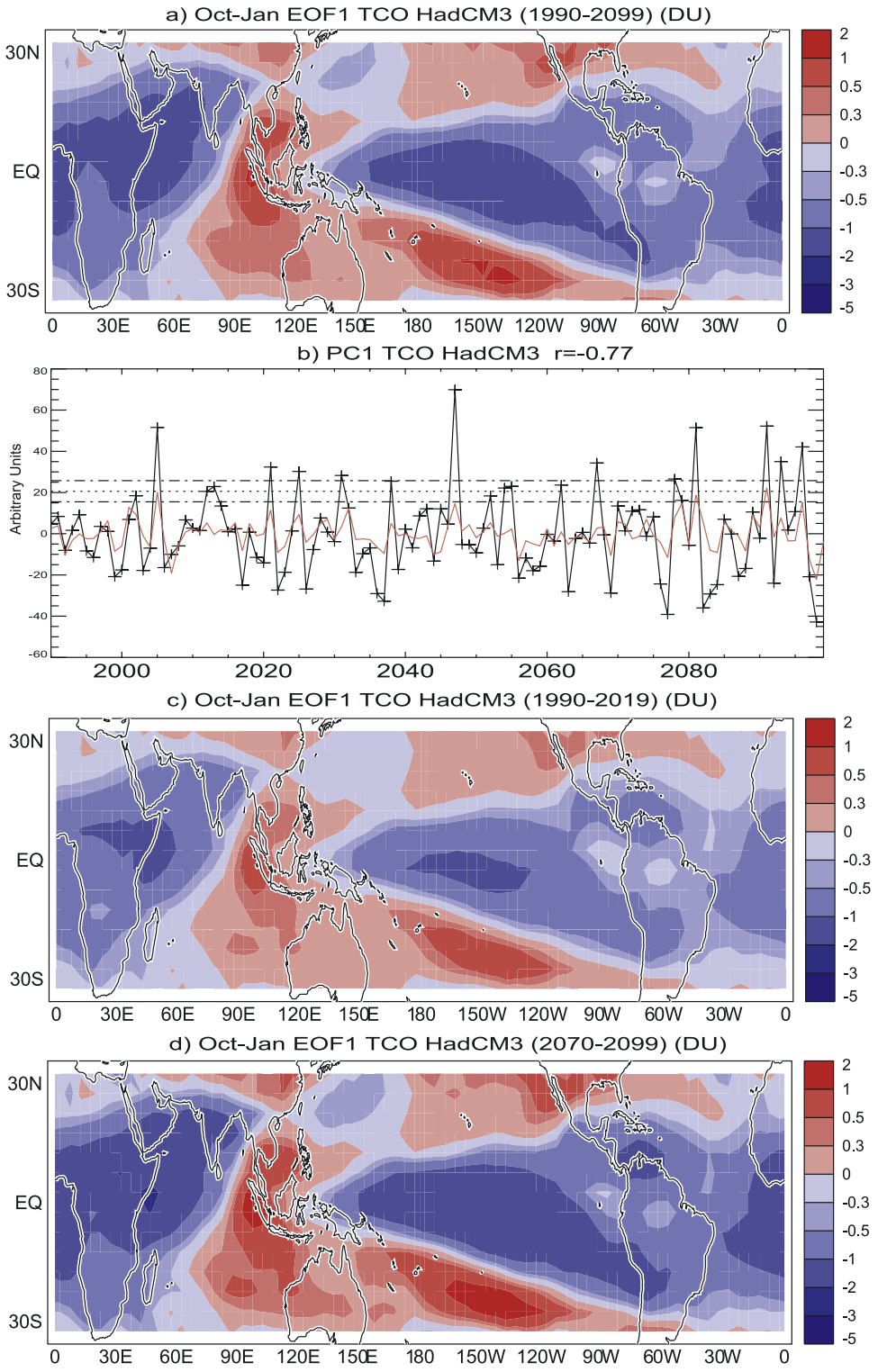

Figure 12. October–January "seasonal" average (a) EOF1 TCO (scaled by +1 standard deviation change of the PC1 time series) 1990–2099 (DU) and (b) PC1 TCO time series (black) (+1 standard deviation of the whole series is depicted by dotted line) and Niño 3 index (red) (r = 0.77). Upper (lower) dot-dashed line is +1 standard deviation for 1990–2019 (2070–2099). (c) EOF1 TCO (scaled by +1 standard deviation of the PC1 time series for 1990–2019; lower dashed line in Figure 12b) (DU) and (d) EOF1 TCO (scaled by +1 standard deviation of the PC1 time series for 2070–2099; upper dashed line in Figure 12b) (DU) for HadCM3 SRES A2 simulation.

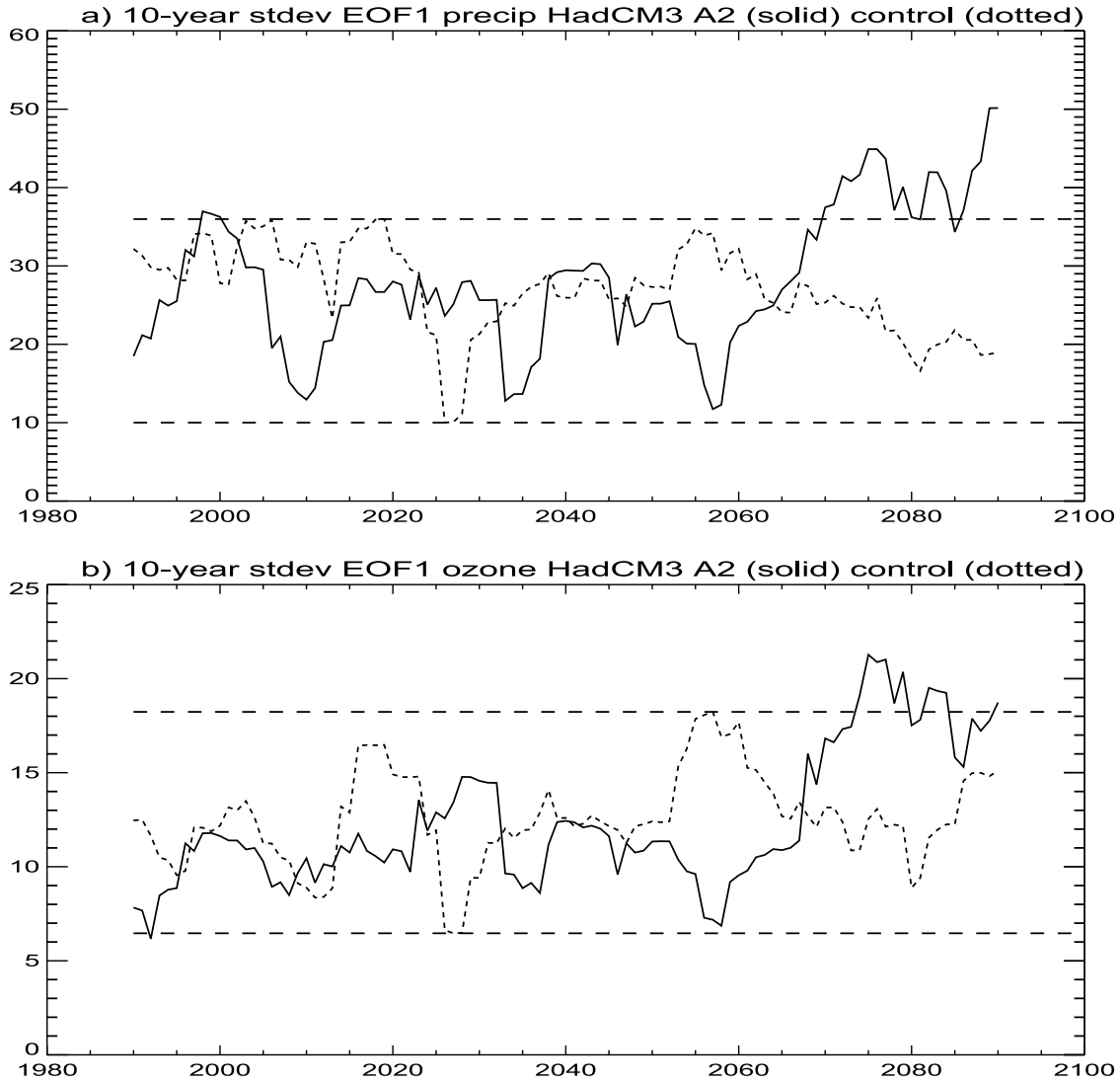

Figure 13. Ten-year running mean standard deviation of annual SRES A2 (solid) and control (dotted): (a) EOF1 precipitation (mm/day) and (b) EOF1 TCO (DU). Maximum and minimum values from the control simulation are depicted as dashed lines.

analysis is performed on October-January average TCO. Therefore we expect the absolute magnitudes may be slightly lower when examining the TCO change during the peak month of change (Figure 4a) versus the peak season of change (Figures 12a and 12c). Comparing Figures 12a and 12c with Figure 4c we see that the negative anomalies are weaker over South America in HadCM3-STOCHEM than in HadAM3-STOCHEM, as lightning NOx emissions are invariant in the former simulation. The convective mixing schemes employed in HadAM3-STOCHEM and HadCM3-STOCHEM models are rather different (section 2.1). The scheme employed in the former model is a Lagrangian type scheme that lifts air parcels in convective updraught and subsides surrounding air parcels, while that in the latter model is a diffusive scheme that uniformly mixes air below the top of a convective cloud [*Collins et al.*, 2002]. Despite these different convective mixing scheme the two model versions of STOCHEM depict similar changes in TCO.

[37] Figure 12 also displays a strong relationship between PC1 TCO and the Niño 3 index in HadCM3-STOCHEM SRES A2 simulation (r = 0.76; Figure 12b). PC1 TCO increases in variability from the mid-2060s unlike in the control simulation (not shown). Figure 13 shows the 10-year running mean interannual standard deviation for precipitation and TCO. The curves display similar characteristics to the SST standard deviation in Figure 10, with similar upward trends from 2060. However, for precipitation and TCO the standard deviations after 2070 exceed the maximum standard deviation from the control simulation. Thus the impact of ENSO on precipitation and TCO strengthens in the future in the SRES A2 simulation as can be seen from a comparison of Figures 12c and 12d.

6. Discussion and Conclusions

[38] The impact of El Niño Southern Oscillation (ENSO) on tropospheric column ozone (TCO) has been examined in

a coupled climate-chemistry model. We obtain similar results to those of previous studies that show negative TCO anomalies over the east/central Pacific and positive TCO anomalies over Indonesia/west Pacific in response to circulation and convective changes during El Niño conditions. However, we underestimate peak positive TCO anomalies over Indonesia and the west Pacific during the peak of the El Niño period. Examining the meteorological impact of El Niño alone on TCO we simulate stronger negative anomalies over South America compared to other studies. These are the result of El Niño–induced reductions in lightning NO_x emissions. Changes in TCO over the central Pacific qualitatively agree with results from a sensitivity experiment that investigates the impact of convective mixing in remote oceanic regions [*Doherty et al.*, 2005]. However, the two cases are not directly comparable, as in the sensitivity study only the impact of convection is considered while during ENSO circulation and convective changes occur. Changes in tropospheric-column average NO_x for El Niño conditions are dominated by the effect of suppressed convection and lightning NO_x emissions over land. This response is quite different from that displayed by *Sudo and Takahashi* [2001] in which the changes in NO_x are qualitatively similar to the changes in ozone and exhibits only a small region of decrease as a result of reduced lightning.

[39] When annually varying biomass burning emissions are included in our simulations we find an enhancement in TCO over Indonesia and South America, although this enhancement in TCO due to biomass burning reaches a maximum before the peak of the dynamical response to ENSO. Thus although increases in TCO occur over these land regions in September and October, the effect of biomass burning has little impact during the peak SST months of December and January. Our simulated enhancement of TCO over Indonesia during the strongest biomass burning month of the 1990s decade (October 1997) was considerably lower than observed or simulated in previous modeling studies. This is at least partly due to an underestimate of the biomass burning emissions anomaly. In agreement with previous studies, the effect of biomass burning over Indonesia was largely confined to a small spatial area and mainly to the LT as a result of suppressed convection.

[40] Finally, the impact of ENSO on TCO in coupled model simulations of future greenhouse gas warming has been examined. A shift in climate toward a future mean El Niño–like state is simulated, as in other studies with the same climate model HadCM3, but this has no discernable impact on mean TCO. Our model does however simulate a future increase in the interannual variability of ENSO-related precipitation and TCO.

[41] A number of outstanding questions still remain and we attempt to provide plausible explanations based on results in this paper and comparison with other literature.

[42] 1. Why are TCO anomalies lower over Indonesia in the case of the meteorological impact of ENSO in this study compared to some previous studies?

[43] TCO anomalies for a normal El Niño event over the west Pacific/Indonesia are comparable with those of *Peters et al.* [2001]. However, for a peak El Niño event TCO anomalies are lower than those found by *Sudo and Takahashi* [2001] and *Chandra et al.* [2002] in October 1997. *Sudo and Takahashi* [2001] use ECMWF reanalyses and *Chandra et al.* [2002] use GEOS data in their simulations. We investigated whether differences between changes in precipitation and water vapor predicted from ECMWF reanalyses versus HadAM3 is the cause of the smaller TCO changes over Indonesia. Both suppressed convection (reduced mixing) and lower water vapor (less ozone destruction) lead to enhanced TCO concentrations over the Indonesian region. Consequently, a smaller decrease in precipitation or humidity in HadAM3 compared to ECMWF reanalyses may result in a smaller simulated TCO increase. We compared changes in convective precipitation and water vapor in HadAM3 with ECMWF reanalyses, over the period October–January 1997/1998–1996/1997. A larger decrease in precipitation (2–5 mm/day) and humidity was generally simulated in HadAM3 compared to ECMWF reanalyses. Therefore the lower ENSO-related TCO anomalies over Indonesia in HadAM3 do not appear to be a result of a lower sensitivity of the hydrological cycle to ENSO in HadAM3. However, we cannot rule out differences in convection mixing schemes as the source of intermodel differences in ENSO-related simulated TCO anomalies over Indonesia in this study compared to previous studies. As an aside, the larger changes in convective precipitation in HadAM3 compared to ECMWF reanalyses are perhaps surprising given the weaker precipitation response displayed in Figure 2 when compared to the CMAP observational data set (also evident when comparing October-January 1997/1998–1997/1996 precipitation in HadAM3 and CMAP).

[44] 2. Why is the TCO increase due to biomass burning smaller compared to other modeling studies?

[45] We do not simulate as large an increase in TCO for a peak El Niño event compared to observational and the modeling study of *Chandra et al.* [2002] of the October 1997 event. For October 1997 we simulate a 4 DU increase in TCO over Indonesia. We find that CO emissions over Indonesia used in our study (that use *Cooke and Wilson* [1996] spatial patterns) are about ½ that of *Duncan et al.* [2003], for October 1997 (that use mainly ATSR seasonal patterns). The latter biomass burning data set was used by *Chandra et al.* [2002]. Large differences even between two satellite-derived data sets: AVHRR and ATSR can be seen over Indonesia in Figure 1 of *Duncan et al.* [2003]. If we assume a linear scaling between emissions and TCO change, using the Duncan et al. emissions for 1997 would increase our CO and NO_x emissions due to biomass burning two-fold yielding TCO increases of ~8 DU for a peak El Niño event, much closer to those observed. Therefore we expect our lower simulated TCO changes due to elevated biomass burning during El Niño are predominantly a result of underestimates in our seasonal biomass burning emissions over Indonesia. Another consideration is that Indonesia has moderate-high anthropogenic emissions of NO_x (up to 1.3 Tg N yr^{-1}). We suspect therefore that with a threefold increase in biomass burning emissions in October 1997 the NO_x production efficiency declines rapidly and thus we do not see as much extra ozone production from biomass burning as assuming a linear response. Lower biomass burning emissions in our control simulation with HadAM3-STOCHEM may also partly explain a lower

ENSO-related TCO increase over Indonesia compared to that simulated in previous model studies. It may also explain the reduction/larger reduction in TCO over Brazil compared to previous studies.

[46] 3. How likely are our future changes in the mean state or amplitude of ozone anomalies due to convective changes?

[47] As discussed earlier, *Collins* [2005] investigated how closely the future trends in SST and precipitation anomalies in the tropical Pacific resembled the ENSO-like interannual signal in these variables in 20 coupled ocean-atmosphere GCMs used in the Coupled Model Intercomparison Project (CMIP). He found that the models with the largest ENSO-like change have the poorest simulation of ENSO variability and calculated that for the CMIP models the most likely scenario was for no trend toward El Niño or La Niña–like conditions. Only a few studies have examined future changes in ENSO variability in climate model simulations of greenhouse gas warming. *Timmermann et al.* [1999] reported an increase in the amplitude of Niño 3 SST anomalies in a future period in a simulation with a 1% increase in greenhouse gases per annum in the ECHAM4 GCM. As discussed earlier *Collins* [2000] and *Collins et al.* [2001] also found an increase in ENSO amplitude in a simulation with quadrupled CO_2 with the HadCM2 but no such increase with HadCM3. Conversely, *Knutson et al.* [1997] simulated a decrease in the amplitude of ENSO under a heightened CO_2 simulation with the GFDL-R15a GCM. Hence there is no overall consensus on possible changes in the amplitude of ENSO in the future. One or two studies have examined EOF1 tropical precipitation and found a strong relationship with ENSO in observations [*Dai and Wigley*, 2000] and in GCMs [*Doherty and Hulme*, 2002]. We do not know of any studies to date that have investigated future changes in the amplitude of ENSO-related precipitation or ozone. However, *Timmermann et al.* [1999] examined the sensitivity of zonal wind stress anomalies to Niño 3 SST anomalies, and found no change in the future despite enhanced Niño 3 SST variability. They concluded that the increased intensity in Niño 3 SST variability in the future was driven by oceanic changes in the ECHAM4 simulation, and that this increased SST variability did not influence atmospheric dynamics. The results of our study shows enhanced SST amplitudes and enhanced ENSO-related precipitation intensity in the future. We also find a significant increase in the sensitivity of ENSO-related precipitation to Niño 3 SST anomalies, as calculated following the method of *Timmermann et al.* [1999]. It would be interesting to see if an increase in the amplitude of ENSO-related precipitation and a corresponding increase in the amplitude of the ozone response is a common feature amongst GCMs and coupled climate-chemistry models. If this is the case, more El Niño events of similar intensity to that of 1997/1998 may be experienced in the future.

[48] **Acknowledgments.** This work was supported by the NERC UTLS thematic programme (NER/T/S/2000/01041). D.S.S. was supported by NERC / Environment Agency advanced fellowship funding (P4-F02, NER/J/S/2000/00840). The UGAMP project is thanked for computing resources to run the coupled HadAM3-STOCHEM model. We would especially like to thank B. Duncan for use of this annually varying biomass burning emissions data set. We also thank J. Jones, M. Widmann, H. Pumphrey and R. Thompson for statistical advice. We thank two anonymous reviewers for their most helpful comments.

References

Chandra, S., J. R. Ziemke, W. Min, and W. G. Read (1998), Effects of 1997–1998 El Niño on tropospheric ozone and water vapour, *Geophys. Res. Lett.*, *25*(20), 3867–3870.

Chandra, S., J. R. Ziemke, P. K. Bhartia, and R. V. Martin (2002), Tropical tropospheric ozone: Implications for dynamics and biomass burning, *J. Geophys. Res.*, *107*(D14), 4188, doi:10.1029/2001JD000447.

Collins, M. (2000), Understanding uncertainties in the response of ENSO to greenhouse warming, *Geophys. Res. Lett.*, *27*(21), 3509–3513.

Collins, M. (2005), El Niño or La Niña-like change, *Clim. Dyn.*, *24*, 89–104.

Collins, M., S. F. B. Tett, and C. Cooper (2001), The internal climate variability of HadCM3, a version of the Hadley Centre coupled model without flux adjustments, *Clim. Dyn.*, *17*, 61–81.

Collins, W. J., R. G. Derwent, C. E. Johnson, and D. S. Stevenson (2002), A comparison of two schemes for the convective transport of chemical species in a Lagrangian global chemistry model, *Q. J. R. Meteorol. Soc.*, *128*, 991–1009.

Cooke, W. F., and J. N. Wilson (1996), A global black carbon aerosol model, *J. Geophys. Res.*, *101*, 19,395–19,409.

Cox, P. M., R. A. Betts, M. Collins, P. P. Harris, C. Huntingford, and C. D. Jones (2004), Amazonian forest dieback under climate-carbon cycle projections for the 21st century, *Theor. Appl. Climatol.*, *78*(1–3), 137–156.

Cubasch, U., G. A. Meehl, G. J. Boer, R. J. Stouffer, M. Dix, A. Noda, C. A. Senior, S. Raper, and K. S. Yap (2001), Projections of future climate change, in *Climate Change 2001: The Scientific Basis—Contribution of WG1 to the Third Assessment Report of the IPCC*, edited by J. T. Houghton et al., pp. 525–582, Cambridge Univ. Press, New York.

Dai, A., and T. M. L. Wigley (2000), Global patterns of ENSO-induced precipitation, *Geophys. Res. Lett.*, *27*(9), 1283–1286.

Dentener, F. D., D. S. Stevenson, J. Cofala, R. Mechler, M. Amann, P. Bergamaschi, F. Raes, and R. G. Derwent (2005), Tropospheric methane and ozone in the period 1990–2030: CTM calculations on the role of air pollutant and methane emissions controls, *Atmos. Chem. Phys.*, *5*, 1731–1755.

Doherty, R., and M. Hulme (2002), The relationship between the SOI and extended tropical precipitation in simulations of future climate change, *Geophys. Res. Lett.*, *29*(10), 1475, doi:10.1029/2001GL014601.

Doherty, R. M., D. S. Stevenson, W. J. Collins, and M. G. Sanderson (2005), Influence of convective transport on tropospheric ozone and its precursors in a chemistry-climate model, *Atmos. Chem. Phys. Disc.*, *5*, 3747–3771.

Duncan, B. N., R. V. Martin, A. C. Staudt, R. Yevich, and J. A. Logan (2003), Interannual and seasonal variability of biomass burning emissions constrained by satellite observations, *J. Geophys. Res.*, *108*(D2), 4100, doi:10.1029/2002JD002378.

Fujiwara, M., K. Kita, S. Kawakami, T. Ogawa, N. Komala, S. Saraspriya, and A. Suripto (1999), Tropospheric ozone enhancements during the Indonesian forest fire events in 1994 and in 1997 as revealed by ground-based observations, *Geophys. Res. Lett.*, *26*(16), 2417–2420.

Fujiwara, M., K. Kita, T. Ogawa, S. Kawakami, T. Sano, N. Komala, S. Saraspriya, and A. Suriputo (2000), Seasonal variation of tropospheric ozone in Indonesia revealed by 5-year ground-based observations, *J. Geophys. Res.*, *105*, 1879–1888.

Gregory, D., R. Kershaw, and P. M. Innes (1997), Parameterization of momentum transport by convection. II: Tests in single-column and general circulation models, *Q. J. R. Meteorol. Soc.*, *123*, 1153–1183.

Johns, T. C., et al. (2003), Anthropogenic climate change for 1860 to 2100 simulated with the HadCM3 model under updated emissions scenarios, *Clim. Dyn.*, *20*, 583–612.

Johnson, C. E., D. S. Stevenson, W. J. Collins, and R. G. Derwent (2002), Interannual variability in methane growth rate simulated with a coupled Ocean-Atmosphere-Chemistry model, *Geophys. Res. Lett.*, *29*(19), 1903, doi:10.1029/2002GL015269.

Knutson, T. R., S. Manabe, and D. Gu (1997), Simulated ENSO in a global coupled ocean-atmosphere model: Multidecadal amplitude modulation and CO_2 sensitivity, *J. Clim.*, *10*, 138–161.

Labrador, L. J., R. von Kuhlmann, and M. G. Lawrence (2005), The effects of lightning-produced NO_x and its vertical distribution on atmospheric chemistry: Sensitivity simulations with MATCH-MPIC, *Atmos. Chem. Phys.*, *5*, 1815–1834.

Li, D., and K. P. Shine (1995), A 4-dimensional ozone climatology for UGAMP models, UGAMP internal report, Univ. of Reading, Reading, U. K.

Nakićenović, N., et al. (2000), *IPCC Special Report on Emissions Scenarios*, 599 pp., Cambridge Univ. Press, New York.

North, G. R., T. L. Bell, R. F. Cahalan, and F. J. Moeng (1982), Sampling errors in the estimation of empirical orthogonal functions, *Mon. Weather Rev.*, *110*, 699–706.

Osborn, T. J. (2004), Simulating the winter North Atlantic Oscillation: The roles of internal variability and greenhouse gas forcing, *Clim. Dym.*, *22*, 605–623.

Peters, W., M. Krol, F. Dentener, and J. Lelieveld (2001), Identification of an El Niño-Southern Oscillation signal in a multiyear global simulation of tropospheric ozone, *J. Geophys. Res.*, *106*(D10), 10,389–10,402.

Pickering, K. E., Y. Wang, W.-K. Tao, C. Price, and J.-F. Muller (1998), Vertical distributions of lightning NO_x for use in regional and global chemical transport models, *J. Geophys. Res.*, *103*(D23), 31,203–31,216.

Pope, V. D., M. L. Gallani, P. R. Rowntree, and R. A. Stratton (2000), The impact of new physical parameterizations in the Hadley Centre climate model: HadAM3, *Clim. Dyn.*, *16*, 123–146.

Prather, M., et al. (2001), Atmospheric chemistry and greenhouse gases, in *Climate Change 2001: The Scientific Basis—Contribution of WG1 to the Third Assessment Report of the IPCC*, edited by J. T. Houghton et al., pp. 239–287, Cambridge Univ. Press, New York.

Price, C., J. Penner, and M. Prather (1997), NO_x from lightning: 1. Global distribution based on lightning physics, *J. Geophys. Res.*, *102*, 5929–5941.

Sanderson, M. G., W. J. Collins, R. G. Derwent, and C. E. Johnson (2003a), Simulation of global hydrogen levels using a Lagrangian three-dimensional model, *J. Atmos. Chem.*, *46*, 15–28.

Sanderson, M. G., C. D. Jones, W. J. Collins, C. E. Johnson, and R. G. Derwent (2003b), Effect of climate change on isoprene emissions and surface ozone levels, *Geophys. Res. Lett.*, *30*(18), 1936, doi:10.1029/2003GL017642.

Stevenson, D. S., W. J. Collins, C. E. Johnson, and R. G. Derwent (1998), Intercomparison and evolution of atmospheric transport in a Lagrangian model (STOCHEM) and an Eulerian model (UM) using 222–Rn as a short-lived tracer, *Q. J. R. Meteorol. Soc.*, *124*, 2477–2491.

Stevenson, D. S., C. E. Johnson, W. J. Collins, R. G. Derwent, and J. M. Edwards (2000), Future tropospheric ozone radiative forcing and methane turnover: The impact of climate change, *Geophys. Res. Lett.*, *27*, 2073–2076.

Stevenson, D. S., R. M. Doherty, M. G. Sanderson, W. J. Collins, C. E. Johnson, and R. G. Derwent (2004), Radiative forcing from aircraft NOx emissions: Mechanisms and seasonal dependence, *J. Geophys. Res.*, *109*, D17307, doi:10.1029/2004JD004759.

Stevenson, D. S., R. M. Doherty, M. G. Sanderson, C. E. Johnson, W. J. Collins, and R. G. Derwent (2005), Impacts of climate change and variability on tropospheric chemistry, *Faraday Disc.*, *130*, 41–58, doi:10.1039/b417412g.

Stevenson, D. S., et al. (2006), Multimodel ensemble simulations of present-day and near-future tropospheric ozone, *J. Geophys. Res.*, *111*, D08301, doi:10.1029/2005JD006338.

Sudo, K., and M. Takahashi (2001), Simulation of tropospheric ozone changes during 1997–1998 El Niño: Meteorological impact on tropospheric photochemistry, *Geophys. Res. Lett.*, *28*(21), 4091–4094.

Thompson, A. M., J. C. Witte, R. D. Hudson, H. Guo, J. R. Herman, and M. Fujiwara (2001), Tropical tropospheric ozone and biomass burning, *Science*, *291*, 2128–2132.

Timmermann, A., J. Oberhuber, A. Bacher, M. Esch, M. Latif, and E. Roeckner (1999), Increased El Niño frequency in a climate model forced by future greenhouse warming, *Nature*, *398*, 694–697.

Valks, P. J. M., R. B. A. Koelemeijer, M. van Weele, P. van Velthoven, J. P. F. Fortuin, and H. Kelder (2003), Variability in tropical tropospheric ozone: Analysis with Global Ozone Monitoring Experiment observations and a global model, *J. Geophys. Res.*, *108*(D11), 4328, doi:10.1029/2002JD002894.

Williams, K. D., C. A. Senior, and J. F. B. Mitchell (2001), Transient climate change in the Hadley Centre models: The role of physical processes, *J. Clim.*, *14*, 2659–2674.

Xie, P., and P. A. Arkin (1996), Analyses of global monthly precipitation using gauge observations, satellite estimates, and numerical model predictions, *J. Clim.*, *9*, 840–858.

Yevich, R., and J. A. Logan (2003), An assessment of biofuel use and burning of agricultural waste in the developing world, *Global Biogeochem. Cycles*, *17*(4), 1095, doi:10.1029/2002GB001952.

Zeng, G., and J. A. Pyle (2005), Influence of El Niño Southern Oscillation on stratosphere/troposphere exchange and the global tropospheric ozone budget, *Geophys. Res. Lett.*, *32*, L01814, doi:10.1029/2004GL021353.

Ziemke, J. R., and S. Chandra (1999), Seasonal and interannual variabilities in tropical tropospheric ozone, *J. Geophys. Res.*, *104*(D17), 21,425–21,442.

Ziemke, J. R., and S. Chandra (2003), La Niña and El Niño—induced variabilities of ozone in the tropical lower atmosphere during 1970–2001, *Geophys. Res. Lett.*, *30*(3), 1142, doi:10.1029/2002GL016387.

W. J. Collins, C. E. Johnson, and M. G. Sanderson, Hadley Centre for Climate Prediction and Research, Met Office, Exeter EX1 3PB, UK.

R. M. Doherty and D. S. Stevenson, Institute of Atmospheric and Environmental Sciences, University of Edinburgh, Edinburgh EH9 3JN, UK. (ruth.doherty@ed.ac.uk)